On the nature and dynamics of the seismogenetic systems of North California, USA: An analysis based on Non-Extensive Statistical Physics

Angeliki Efstathiou[1], Andreas Tzanis[1] and Filippos Vallianatos[2]

[1] *National and Kapodestrian University of Athens, Department of Geophysics and Geothermy, Panepistimiopoli, Zografou 15784, Greece; e-mail: aefstathiou@geol.uoa.gr; atzanis@geol.uoa.gr.*

[2] *Laboratory of Geophysics and Seismology & UNESCO Chair on Solid Earth Physics and Geohazards Risk Reduction, Technological Educational Institute of Crete, Chania, GR 73133, Crete, Greece. e-mail: fvallian@chania.teicrete.gr*

Appears in:

Physics of the Earth and Planetary Interiors, 270 (2017) 46–72; doi: http://dx.doi.org/10.1016/j.pepi.2017.06.010

Athens, June 2017

Abstract

We examine the nature of the seismogenetic system in North California, USA, by searching for evidence of complexity and non-extensivity in the earthquake record. We attempt to determine whether earthquakes are generated by a self-excited Poisson process, in which case they obey Boltzmann-Gibbs thermodynamics, or by a Critical process, in which long-range interactions in non-equilibrium states are expected (correlation) and the thermodynamics deviate from the Boltzmann-Gibbs formalism. Emphasis is given to background seismicity since it is generally agreed that aftershock sequences comprise correlated sets. We use the complete and homogeneous earthquake catalogue published by the North California Earthquake Data Centre, in which aftershocks are either included, or have been removed by a stochastic declustering procedure. We examine *multivariate* cumulative frequency distributions of earthquake magnitudes, interevent time and interevent distance in the context of Non-Extensive Statistical Physics, which is a generalization of extensive Boltzmann-Gibbs thermodynamics to non-equilibrating (non-extensive) systems. Our results indicate that the seismogenetic systems of North California are generally sub-extensive complex and non-Poissonian. The background seismicity exhibits long-range interaction as evidenced by the overall increase of correlation observed by declustering the earthquake catalogues, as well as by the high correlation observed for earthquakes separated by long interevent distances. It is also important to emphasize that two subsystems with rather different properties appear to exist. The correlation observed along the Sierra Nevada Range – Walker Lane is quasi-stationary and indicates a Self-Organized Critical fault system. Conversely, the north segment of the San Andreas Fault exhibits changes in the level of correlation with reference to the large Loma Prieta event of 1989 and thus has attributes of Critical Point behaviour albeit without acceleration of seismic release rates. SOC appears to be a likely explanation of complexity mechanisms but since there are other ways by which complexity may emerge, additional work is required before assertive conclusions can be drawn.

Key words: Non-extensive Statistical Physics; Complexity; Seismicity; North California; San Andreas Fault; Walker Lane.

1. Introduction

It is generally accepted that the observed seismicity comprises a *background process* that expresses the continuum of tectonic deformation at a given active fault system (seismogenetic area), which is draped by a large population of triggered events and aftershock sequences that express short-term activity associated with background events (*foreground process*). Although, progress has been made towards understanding the foreground process, the statistical physics of background seismicity, hence the way in which seismicity and tectonic deformation evolve, has not been clarified with significant repercussions on problems pertaining to hazard analysis and long-term forecasting.

The development of theoretical and experimental models that combine the physics and statistics of seismogenesis has led to two general theoretical contexts (viewpoints) as to the nature of background seismicity. Of those, the first and currently most influential viewpoint postulates that the expression of the background process is Poissonian in time and space (point process) and obeys Boltzmann-Gibbs thermodynamics. The second postulates that seismogenesis is a Complex process and involves some form of criticality, (e.g. stationary or self-organized vs. evolutionary or self-organizing), although non-critical models which maintain the seismogenetic system in a perennial state of non-equilibrium have also been proposed.

The present study is part of a systematic attempt to examine the statistical nature and the dynamics of seismogenetic systems by using the generalized description of *both* Poissonian and Complex systems afforded by the theoretical framework of Non Extensive Statistical Physics (NESP) and searching for signs of randomness or self-organization in time and in space. The remaining of this presentation is organized as follows: In Section 1.1 we provide an overview of the two prevalent viewpoints and in Section 1.2 we explain the rationale on which we based our research. Section 2.1 provides a brief exposé of non-extensive Statistical Physics and Section 2.2 deals with its implementation. The analysis focuses on the seismicity of North California, U.S., as this is a very well-studied area with reliable earthquake monitoring services and seismological catalogues. A brief presentation of the geotectonic context and a thorough presentation of the data (earthquake catalogues) and the data reduction and analysis procedures is given in Section 3. Section 4 is devoted to the presentation of the results and the validation/verification tests conducted to appraise their rigour. Finally, in Section 5 it is argued that the statistical nature of earthquake occurrence in North California is best described by power-laws consistent with NESP and that the seismicity is likely generated by a Self-Organized Critical fault system

1.1. Brief overview of Earthquake Statistics: Randomness vs. Complexity.

Paradigmatic expression of the "Poissonian viewpoint" is the ETAS model (Episodic Type Aftershock Sequence, e.g. Ogata, 1988, 1998; Zhuang et al, 2002; Helmstetter and Sornette, 2003; Touati et al, 2009; Segou et al, 2013). This is an empirical construct which essentially expresses a self-excited conditional Poisson process (Hawkes, 1972; Hawkes and Adamopoulos, 1973; Hawkes and Oakes, 1974). According to ETAS, random background main events trigger aftershock sequences in which aftershocks trigger their own sub-sequences thus leading to short-term spatiotemporal clustering of multiple generations of foreground events whose overall time dependence is described by a power law known as the Omori-Utsu law (e.g. Utsu et al., 1995). Point process models have also been developed to address the problem of intermediate to long-term clustering such as the EEPAS (Each Earthquake is a Precursor According to

Scale, e.g. Rhoades, 2007) and the PPE (Proximity to Past Earthquakes, e.g. Marzocchi and Lombardi, 2008). Point processes are memoryless, therefore the Poissonian viewpoint rests on the assumption that background earthquakes are statistically independent and although it is possible for any one event to trigger another, this occurs in an unstructured random fashion and does not contribute to the long-term evolution of seismicity. It is important to emphasize that the Poissonian viewpoint is mainly concerned with the statistics of time and distance between earthquake events; the size (magnitude) distribution of both background and foreground processes is still thought to be governed by the well-established frequency – magnitude (F-M) relationship of Gutenberg and Richter. It follows that a weakness (if not inconsistency) of this viewpoint is that the scale-free grading between earthquake frequency and magnitude implied by the F-M relationship *cannot* be derived from the Boltzmann-Gibbs formalism.

The "Complexity viewpoint" is also model-driven, which may be the reason why the types and mechanisms of complexity have not been clarified as yet. A well-studied class of models (Bak and Tang, 1989; Sornette and Sornette, 1989; Olami et al., 1992; Bak et al., 2002; Caruso et al., 2007; Bakar and Tirnakli, 2009; Hergarten and Krenn, 2011; many others) suggests that seismicity expresses a non-equilibrating fractal fault system that continuously evolves toward a stationary critical condition with no characteristic spatiotemporal scale (Self Organized Criticality – SOC). In this view, all earthquakes belong to, or evolve towards the same global population and participate in shaping a non-equilibrium state in which events develop spontaneously and any small instability has a chance of cascading into a large shock. A second class of models which have been rather influential during the late 1990's and 2000's, suggest that the evolution of seismicity prior to large events expresses a Critical Point (or Self-Organizing Critical) process (e.g. Sornette and Sammis, 1995; Rundle et al., 2000; Sammis and Sornette, 2001; many others). In this view, tectonic loading combined with stress transfer from smaller events establishes long range stress correlation and produces acceleration of energy release rates in a power-law fashion, until the network has reached a critical state with correlation extending over the scale of the network so that a local event can grow by rupturing through geometrical and rheological barriers. At any rate, critical complex systems evolving in a fractal-like space-time are characterized by long-range interactions and long-term memory which, at a regional scale, should be manifested by correlations and power-law distributions observable in the statistical behaviour of their energy release, temporal dependence and spatial dependence. In addition to the Critical, a few authors have investigated models with alternative complexity mechanisms that do not involve criticality, yet maintain the fault system in a state of non-equilibrium: a useful discussion can be found in Sornette and Werner (2009). More recently, Celikoglu et al, (2010) applied the Coherent Noise Model (Newman, 1996) based on the notion of external stress acting coherently onto all agents of the system without having any direct interaction with them and is shown to generate power-law interevent time distributions. A weak point in this model is that it does not include some geometric configuration of the agents and it is not known how this would influence the behaviour of the system. In another example, Mignan (2008) has formulated the "non-critical Precursory Accelerating Seismicity Theory" which behaves similarly to a CP process; in this context, stress correlation is a result of top-down tectonic loading due to a large-scale preparation process and not bottom-up triggering as predicted by the CP theory.

Both Poissonian and Complexity/Criticality models agree that the foreground process (aftershocks) comprises a set of dependent events, but whereas the former assign only local significance to this dependence, Criticality considers them to be an integral part of the regional seismogenetic process. The

fundamental difference between the Poissonian and Criticality viewpoints is in their understanding of the background process. The former implicitly assumes that there is no correlation (interaction) between background events, so that the statistical description of their temporal and spatial evolution would be consistent with the Boltzmann-Gibbs thermodynamic formalism. Criticality requires short and long-range interactions in a non-equilibrium state, which beget *correlation* between background/background, background/foreground and foreground/foreground events, endow the fault system with memory and compel power-law behaviour on the statistics of the parameters pertaining to its temporal and spatial evolution.

1.2. Searching for evidence of Randomness vs. Complexity

A natural conclusion of the above discussion is that if it would be possible to identify and remove the foreground process (aftershocks), it might also be possible to inquire the properties of the background process by examining its spatiotemporal characteristics for the existence of correlation. It should be apparent that in order to successfully pursue this line of inquiry one must be equipped with: a) Statistical Physics that comprise a *natural* (not model-based) general context by which to test for the existence of correlation, b) effective measures of correlation in the temporal and spatial expression of seismicity, and, c) effective ways to distinguish between the background and the foreground processes. As it turns out, there are satisfactory (or nearly satisfactory) answers to all three prerequisites.

The advent of Non-Extensive[1] Statistical Physics (NESP) has afforded a fundamental generalized conceptual framework by which to study *non-additive* (non-equilibrating) physical and natural systems in which the total (systemic) entropy is not equal to the sum of the entropies of their components. It has been developed by Tsallis (1988, 2009) as a generalization of the (additive) Boltzmann-Gibbs formalism of thermodynamics and comprises an appropriate tool for the analysis of complexity evolving in a fractal-like space-time and exhibiting scale invariance, long-range interactions and long-term memory (e.g. Gell'mann and Tsallis, 2004). NESP predicts power-law cumulative probability distributions for non-extensive dynamic systems, which reduce to the exponential cumulative distribution in the limiting case of extensive (random/point) processes. NESP has recently been applied to the statistical description of earthquake occurrence with notable results (see Section 2.2) and has also been shown to generate the Gutenberg-Richter frequency-magnitude distribution, which is indeed a power-law, from first principles (e.g. Sotolongo-Costa and Posadas, 2004; Silva, 2006; Telesca, 2011, 2012). Thus, NESP provides a general, complete, consistent and *model-independent* theoretical context in which to investigate the nature and dynamics of the background and foreground seismogenetic processes.

Now, consider that a definite indicator of correlation (interaction) between faults is the lapse between consecutive earthquakes above a magnitude threshold and over a given area: this is variably referred to as *interevent time, waiting time, calm time, recurrence time* etc. Understanding the properties (statistics) of the earthquake frequency – interevent time (F-T) distribution is apparently indispensable for understanding the dynamics of the seismogenetic system and for that reason they have been studied by several researchers. Empirical F-T distributions generally exhibit power-law behaviour and long tails. It

[1] The term *"extensive"* (full or complete according to Merriam-Webster's definition), has been introduced by Tsallis (1988) to designate systems that are equilibrating as opposed to systems that are not equilibrating (incomplete, i.e. *non-extensive*). The terms "*additive*" and "*non-additive*" are probably better suited to designate entropic states but for the sake of consistency we will adhere to Tsallis's definitions.

should, however, be emphasized that hitherto studies have generally focused on the mixed background/foreground processes and not on the background process independently. In the context of Extensive Statistical Physics, F-T distributions have been investigated with different standard statistical models with tails, reducible to power laws in some way or another. Examples of this approach are the gamma distribution and the Weibull distribution (e.g. Bak et al., 2002; Davidsen and Gold, 2004; Corral, 2004; Martinez et al, 2005; Talbi and Yamazaki, 2010). Corral (2004) has applied the gamma distribution and has suggested universality analogous to the Gutenberg–Richter F-M distribution, to which other investigators objected on the basis of self-exciting conditional Poisson models, with some of them proposing *ad hoc* mechanisms for the generation of power laws from the combination of correlated aftershock and uncorrelated background processes (e.g. Saichev and Sornette, 2013; Hainzl et al, 2006; Touati et al, 2009). Notably, Molchan (2005) has shown that for a stationary point process, if there is a universal distribution of interevent times, then it must be exponential! Investigations performed in the context of Non Extensive Statistical Physics will be reviewed in Section 2.2. An analogous measure of fault interaction is the *hypocentral distance* between consecutive earthquakes, above a magnitude threshold and over a given area (*interevent distance*). Apparently, the statistical properties of the earthquake frequency – interevent distance (F-D) distribution should be related to the *range of interaction* over that area. Unfortunately, with less than a handful of attempts to investigate it, (e.g. Eneva and Pavlis, 1991; Abe and Suzuki, 2003; Batac and Kantz, 2014; Shoenball et al., 2015), the statistics of F-D distributions is practically terra incognita. Finally, a common criterion of scaling in earthquake size is the Gutenberg–Richter F-M distribution, which is interpreted to express the scale-free statistics of a fractal active fault system. The F-M distribution is *static* and does not say much about the dynamics of the active fault network. It also says nothing about correlations in the energy released by a given earthquake, with the energy released by its predecessor or successor events. Nevertheless, this undisputable empirical relationship is a yardstick against which to compare any physical and statistical description of the relationship between earthquake size and frequency and as such will be used herein.

The discrimination between background and foreground processes is referred to as *declustering*. Methods of declustering have evolved from deterministic (e.g. Gardner and Knopoff, 1974; Reasenberg, 1985) to stochastic (e.g. Zhuang et al., 2002; Marsan and Lengliné, 2008). An excellent review is provided by van Stiphout et al, (2012). The former methods identify aftershocks using temporal and spatial windows that usually depend on the main shock magnitude while ignoring aftershocks of aftershocks (higher order events). The latter allow for aftershock triggering within a cluster and use Omori's law as a measure of the temporal dependence of aftershock activity. Both approaches ignore fault elongation for larger magnitude events, assuming circular (isotropic) spatial windows. Stochastic declustering was pioneered by Zhuang et al. (2002) and is based on space-time branching approaches to describe how each event triggers its successors. It improves on previous methods in that the choice of space-time distance is optimized by fitting an ETAS model to the earthquake data. Moreover, instead of associating an aftershock with one main shock, each earthquake is assigned with a probability that it is an aftershock of its predecessor. This means that all earthquakes are possible main shocks to their short-term aftermath and neatly circumvents the problem of having to make committing binary decisions in the frequent cases of nearly equal space-time distances between successive events. Marsan and Lengliné (2008) carried stochastic declustering one step forward by introducing a generalized triggering process without a specific underlying earthquake occurrence model, although they still assume that background earthquakes occur at constant and spatially

uniform rate density. Herein we have chosen to implement the stochastic declustering method of Zhuang et al (2002). As will be further elaborated in Section 3, this has a significant for our purpose advantage: it comprises a *paradigmatic* realization of the self-excited Poisson process. Accordingly, if the background seismicity obeys Boltzmann-Gibbs statistics, then this method should be able to extract a nearly random background process against which to test the alternative hypotheses (Complexity/Criticality). If it is does not, the argument in favour of a complex background would be stronger.

2. A Non Extensive Approach to the Statistical Physics of Earthquakes

2.1. Brief introduction to NESP.

Let x be a dynamic parameter of a complex system and $p(x)dx$ the probability of finding its value in $[x, x+dx]$ so that integrating over the total number of the microscopic configurations (states) of the system $\int_0^\infty p(x)dx = 1$. In seismogenetic systems x can be the interevent time, interevent distance, fault and fragment surface, energy etc.

Non-equilibrium states in systems with complex behaviour can be described by the Tsallis (1988) entropic functional:

$$S_q(p) = \frac{k}{q-1}\left[1 - \int_0^\infty p^q(x)dx\right], \quad (1)$$

where k is the Boltzmann constant and q the *entropic index*. In the limiting case $q \to 1$, Eq. (1) converges to the Boltzmann–Gibbs entropy

$$\lim_{q\to 1} S_q(p) = -k\int_0^\infty p(x)\ln[p(x)]dx$$

The Tsallis and Boltzmann-Gibbs entropies share properties such as concavity and fulfilment of the *H*-theorem. However, the Tsallis entropy is not additive when $q \neq 1$, so that it is generally not equal to the sum of the entropies of the elements of the system. Thus, for a mixture of two statistically independent systems *A* and *B*, the Tsallis entropy satisfies

$S_q(A, B) = S_q(A) + S_q(B) + (1-q)\, S_q(A)\, S_q(B)$.

This property is known as *pseudo-additivity* and is further distinguished into *super-additivity* (*super-extensivity*) if $q < 1$, *additivity* when $q \to 1$ (i.e. Boltzmann-Gibbs statistics) and *sub-additivity* (*sub-extensivity*) if $q > 1$. Accordingly, the entropic index is a measure of *non-extensivity* in the system.

An additional feature of non-extensive statistical physics is the generalization of the expectation value in accordance with the generalization of entropy. Thus, the *q-expectation* value of x is defined as

$$\langle x\rangle_q = \int_0^\infty x \cdot p_q(x)dx \quad (2)$$

where $p_q(x)$ is an *escort distribution* defined as

$$p_q(x) = \frac{[p(x)]^q}{\int_0^\infty [p(x')]^q dx'}. \quad (3)$$

The concept of escort distributions has been introduced by Beck and Schloegl (1993) as a means of exploring the structures of (original) distributions describing fractal and multi-fractal non-linear dynamic

systems: the parameter q behaves as a microscope for exploring different regions of $p(x)$ by amplifying the more singular regions for $q > 1$ and the less singular regions for $q < 1$.

Maximization of the Tsallis entropy yields the probability density function (PDF):

$$\hat{p}(x) = \frac{1}{Z_q} \exp_q \left[-\frac{\lambda}{I_q} \left(x - \langle x \rangle_q \right) \right], \tag{4}$$

$$Z_q = \int_0^\infty \exp_q \left[-\frac{\lambda}{I_q} \cdot \left(x - \langle x \rangle_q \right) \right] dx ,$$

$$I_q = \int_0^\infty [\hat{p}(x)]^q \, dx$$

where λ is an appropriate Lagrange multiplier associated with the constraint on the q-expectation value and $\exp_q(.)$ denotes the *q-exponential* function

$$\exp_q(z) = \begin{cases} (1 + (1-q)z)^{\frac{1}{1-q}} & 1 + (1-q)z > 0 \\ 0 & 1 + (1-q)z \le 0 \end{cases}, \tag{5}$$

which comprises a generalization of the exponential function: for $q \to 1$, $\exp_q(z) \to e^z$.

Eq. (4) defines a *q-exponential distribution* and as evident from Eq. (5), $\hat{p}(x)$ is a power-law with (long) tail if $q > 1$, corresponding to *sub-extensivity*, an exponential if $q \to 1$, corresponding to *extensivity* and a power-law with *cut-off* if $0 < q < 1$, corresponding to *super-extensivity*; the cut-off appears at

$$x_c = \frac{x_0}{1-q}, \qquad x_0 = I_q \lambda^{-1} + (1-q)\langle x \rangle_q . \tag{6}$$

Using the definitions of x_0 from Eq. (6) and the q-expectation value from Eq. (3), the probability $\hat{p}(x)$ can be expressed as

$$\hat{p}(x) = \frac{\exp_q \left(x / x_0 \right)}{\int_0^\infty \exp_q \left(x' / x_0 \right) dx'} \tag{7}$$

In the NESP formalism, the theoretical distribution to be fitted to the observed (empirical) distribution of

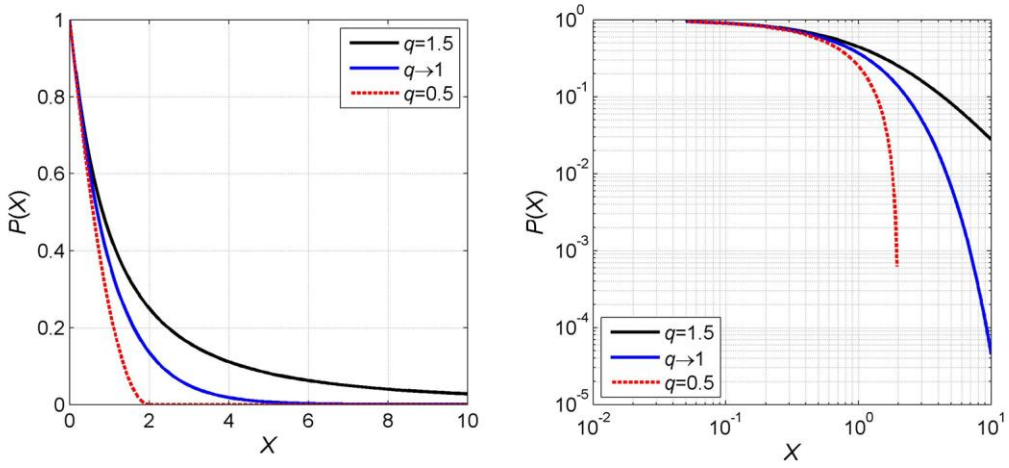

Figure 1. Examples of the q-exponential CDF for different values of q, plotted in linear scale (left) and double-logarithmic scale (right).

x is not the original stationary distribution $\hat{p}(x)$ but the escort probability $\hat{p}_q(x)$. On this premise, the *cumulative* probability function (CDF) is simply:

$$\hat{P}(>x) = \int_x^{\infty} \hat{p}_q(x')dx' . \quad (8)$$

On substituting Eq. (7) in Eq. (3), the CDF reduces to:

$$\hat{P}(>x) = \exp_q\left(-\frac{x}{x_0}\right) = \left[1-(1-q)\left(\frac{x}{x_0}\right)\right]^{\frac{1}{1-q}} \quad (9)$$

which also a q-exponential distribution. For $q > 1$, Eq. (9) defines a CDF of the Zipf-Mandelbrot kind.

Fig. 1 illustrates the q-exponential CDF for different values of q. For $q > 1$ the CDF has a tail that becomes longer (fatter) with increasing q, which translates to increasing correlation and longer term memory. For $q \to 1$, the power law converges to the common exponential distribution so that the system comprises an uncorrelated and memoryless point (random) process. For $0 < q < 1$, the CDF exhibits a cut-off whenever the argument becomes negative, i.e. $\hat{P}(>x) = 0$, and is characterized by a bounded correlation radius.

2.2. Implementation

The Non-Extensive Statistical Physics (NESP) approach has attracted growing attention during the past few years (e.g. Vallianatos and Telesca, 2012) with several researchers studying the properties of the F-T and F-M distributions. A recent comprehensive review of NESP applications to earthquakes and tectonics is given by Vallianatos et al., (2016). The empirical application of NESP to interevent times has been taken up by a handful of authors and the CDF specified by Eq. (9) is the only NESP formulation developed and applied to the analysis of the one-dimensional F-T distributions. The emergence of q-exponential distributions in critical seismicity models was investigated by Caruso et al (2007) and Bakar and Tirnakli (2009), while the same for non-critical models was investigated by Celikoglu et al (2010). In a series of empirical studies, Abe and Suzuki (2005) investigated the temporal statistics of the seismicity in California and Japan, Carbone et al. (2005) in Italy and Darooneh and Dadashinia (2008) in Iran. More recently, Vallianatos et al. (2012a) investigated the spatiotemporal properties of the 1996 Aigion (Greece) aftershock sequence, Vallianatos et al. (2013a) the temporal behaviour of the 2011-2012 seismicity crisis in the Santorini volcanic complex (Greece), Vallianatos et al. (2013b) the spatiotemporal properties of the 2003 Lefkada aftershock sequence, Vallianatos and Sammonds (2013) the behaviour of global seismicity prior to the 2004 Sumatran and 2011 Honsu mega-earthquakes and Papadakis et al., (2015) the 1995 spatiotemporal properties of the 1995 Kobe, Japan, event. Papadakis et al. (2013), Michas et al. (2013), and Antonopoulos et al. (2014) have also published evidence of non-extensive spatiotemporal behaviour in Greek seismicity. In these empirical studies, the F-T distributions $P(>\Delta t)$ were effectively fitted with a one-dimensional q-exponential.

Non-extensive formulations of the frequency-magnitude distribution have been developed by Sotolongo-Costa and Posadas (2004), Silva et al. (2006), Darooneh and Mehri (2010) and Telesca (2011, 2012); these authors introduced frequency-magnitude CDFs which are variations on the same theme more or less, and reduce to the Gutenberg-Richter law as a particular case. Sotolongo-Costa and Posadas (2004) proposed a model for the earthquake generation mechanism that considers the interaction of two rough fault walls and the fragments filling space between them, where the fragments are produced by the local breakup of the material comprising the fault walls (the fragment-asperity model); this interaction is

supposed to modulate earthquake triggering. In this model, the F-M distribution is approached by considering the size distribution of fragments and asperities and the scaling of size with energy, where size is represented by the *relative area* σ, i.e. the area of fragments and asperities normalized by some characteristic value for the area of the fragment-asperity system. The transition from the size distribution to energy and magnitude distributions depends on how energy scales with size and with magnitude.

Sotolongo-Costa and Posadas (2004) assume that the energy stored in the asperities and fragments scales with their linear characteristic dimension ($E \propto r \Rightarrow E \propto \sigma^{1/2}$), and that the magnitude scales with the logarithm of the energy as $M \propto \log(E)$. Darooneh and Mehri (2010) expand on the same model but assume that $E \propto \exp(\sigma^{1/a})$ and $M \propto \ln(E)$. We propose that the above assumptions are not compatible with established ken on earthquake mechanics and the empirical laws of energy – moment and moment – magnitude scaling in particular (e.g. Scholz, 2002; Lay and Wallace, 1995).

Silva et al. (2006) revisited the fragment-asperity model and expressed Eq. (7) as

$$\hat{p}(\sigma) = \left[1 - \frac{1-q}{2-q}\left(\sigma - \langle\sigma\rangle_q\right)\right]^{\frac{1}{1-q}}. \tag{10}$$

On assuming that the energy scales with the characteristic volume of the fragments ($E \propto r^3$), so that $E \propto \sigma^{3/2}$ because σ scales with r^2, it is easy to see that $(\sigma - \langle\sigma\rangle_q) = (E/\alpha)^{2/3}$ with α being a proportionality constant between E and r. This yields the energy density function (EDF)

$$\hat{p}(E) = \left(\frac{2}{3}\cdot\frac{E^{-1/3}}{\alpha^{2/3}}\right)\cdot\left[1 - \frac{(1-q)}{(2-q)}\frac{E^{2/3}}{\alpha^{2/3}}\right]^{-\frac{1}{1-q}}$$

The corresponding CDF is, then,

$$\hat{P}(>E) = \frac{N(>E)}{N_0} = \int_E^{\infty}\hat{p}(E)dE \tag{11}$$

where $N(>E)$ is the number of events with energy greater than E normalized by the total number of earthquakes N_0. On assuming that the magnitude scales with the logarithm of energy as $M \propto \frac{1}{3}\log(E)$, for $q > 1$, Eq. (11) yields

$$\hat{P}(>M) = \frac{N(>M)}{N_0} = \left(1 - \frac{1-q_M}{2-q_M}\cdot\frac{10^{2M}}{\alpha^{2/3}}\right)^{\left(\frac{2-q_M}{1-q_M}\right)} \tag{12}$$

This model has been applied to the analysis of regional seismicity in different tectonic regions (Telesca 2010a, 2010b; Telesca and Chen, 2010; Scherrer et al., 2015). Finally, assuming $E \propto r^3$ but that the magnitude scales with energy as $M \propto \frac{2}{3}\log(E)$, Telesca (2011, 2012) has introduced a modified version of Eq. (12):

$$\hat{P}(>M) = \frac{N(>M)}{N_0} = \left(1 - \frac{1-q_M}{2-q_M}\cdot\frac{10^{M}}{\alpha^{2/3}}\right)^{\left(\frac{2-q_M}{1-q_M}\right)}. \tag{13}$$

We postulate that Telesca's assumption of magnitude – energy scaling, which essentially says that the energy released in the form of seismic waves scales with the effective area of the fault (fragments and asperities), is consistent with the empirical laws of energy–moment and moment–magnitude scaling, as well as compatible with the well-studied rate-and-state friction laws of rock failure. Accordingly, in the ensuing analysis we implement the F-M distribution specified by Eq. (13).

As mentioned in the introduction, our goal is to investigate whether seismicity is a complex/critical or self-excited random (Poisson) process, using the NESP formalism to search for evidence of correlation in time, size and space by determining the values and variation of the relevant entropic indices. The earthquake occurrence model we implement herein will be based on *multivariate* frequency distributions that express the joint probability of observing an earthquake larger than a given magnitude, after a given lapse time and beyond a given distance. However, this would require the construction and analysis of *tri-variate* F-M-T-D distributions (frequency – magnitude – interevent time – interevent distance) which would arguably be harder to handle and interpret. Instead, at this exploratory stage we decided to use easier to study *bivariate* F-M-T distributions in order to inquire for correlation in earthquake size and time of occurrence (memory). This, nonetheless, will not extract direct information about the range of correlation and as a way around this problem we will use the *interevent distance* as a spatial filter by which to separate and study the temporal correlation of *proximal* and *distal* earthquakes: the premise is that if distal earthquakes are correlated in time, then they have to be correlated in space via long-distance interaction and vice versa. The technical details of this approach will now be specified.

2.3. The Frequency–Magnitude–Interevent Time (F-M-T) distribution: Construction and modelling

A bivariate F-M-T distribution that expresses the joint probability of observing an earthquake larger than a given magnitude after a given time lapse (interevent time) can be constructed thus: A *threshold* (cut-off) magnitude M_{th} is set and a bivariate frequency table (histogram) representing the observed *incremental* distribution is first compiled; the observed *cumulative* distribution is then obtained by backward bivariate summation, according to the scheme

$$N_{m\tau} = \sum_{j=D_T}^{\tau} \sum_{i=D_M}^{m} \left\{ H_{ij} \Leftrightarrow H_{ij} \neq 0 \right\}, \quad \tau = 1,\ldots D_T, \quad m = 1,\ldots D_M \tag{14}$$

where H is the incremental distribution, D_M is the dimension of H along the magnitude axis and D_T is the dimension of H along the Δt axis. In this construct, the cumulative frequency (earthquake count) can be written thus: $N(\{M \geq M_{th}, \Delta t : M \geq M_{th}\})$. Then, the empirical probability $P(>\{M \geq M_{th}, \Delta t : M \geq M_{th}\})$ is simply

$$\frac{N\left(>\{M \geq M_{th},\ \Delta t : M \geq M_{th}\}\right)}{N_0}, \qquad N_0 = N(M = M_{th}, 0) = \left\| N \right\|_{\infty}. \tag{15}$$

An example of cumulative FMT distribution constructed according to Eq. (14) is presented in Fig. 2; it is based on the NCSN catalogue published by the North California Earthquake Data Center for the period 1975-2012 and M_{th} = 3.4 (3,653 events excluding the Mendocino Triple Junction and Garlock fault areas – details are given in Section 3). The distribution is illustrated both in linear and logarithmic frequency scales (Figs. 2a and 2b respectively). Apparently, it comprises a well-defined and structured surface, with the end-member at ($M \geq M_{th}$, Δt=0) comprising the one-dimensional Gutenberg – Richter law and the opposite end member at ($M = M_{th}$, Δt) comprising the one-dimensional F-T distribution.

Assuming that the magnitude and interevent time are statistically independent, namely that the hierarchy of the active fault network does not influence the sequence of events, the joint probability $P(M \cup \Delta t)$ may factorize into the probabilities of M and Δt in the sense $P(M \cup \Delta t) = P(M)\ P(\Delta t)$. Then, by implicitly *identifying* the empirical and escort probabilities we obtain

$$\frac{N\left(>\{M \geq M_{th},\ \Delta t : M \geq M_{th}\}\right)}{N_0} = \left(1 - \frac{1-q_M}{2-q_M} \cdot \frac{10^M}{\alpha^{2/3}}\right)^{\left(\frac{2-q_M}{1-q_M}\right)} \cdot \left(1 - (1-q_T) \cdot \frac{\Delta t}{\Delta t_0}\right)^{\frac{1}{1-q_T}}, \tag{16}$$

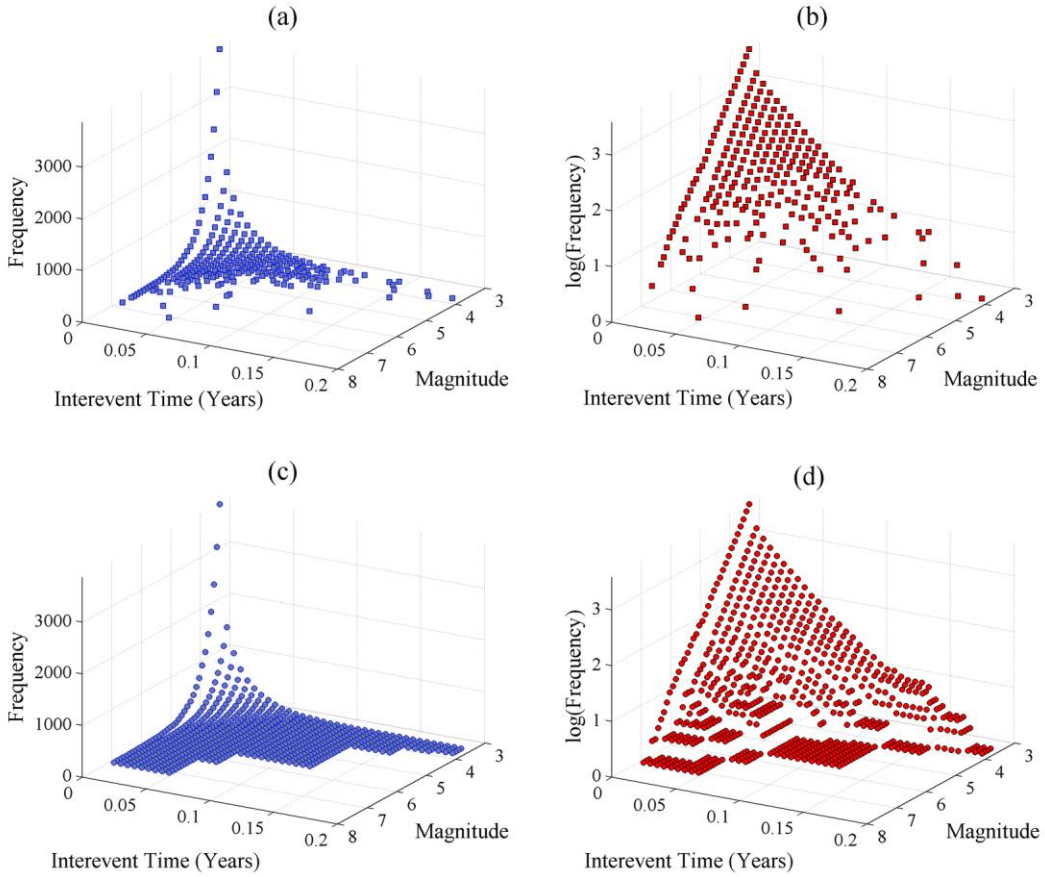

Figure 2. (A) The bivariate cumulative frequency – magnitude – interevent time distribution constructed according to Eq. (14) for the period 1975-2012 and M_{th} = 3.4 on the basis of the homogenized NCSN catalogue (3,653 events excluding the Mendocino Triple Junction and Garlock fault areas; see Section 3 for detils). **(B)** As per (A) but in logarithmic frequency scale. **(C)** As per (A) but including unpopulated bins in the summation, i.e. using the scheme $N_{m\tau} = \sum_{j=D_T}^{\tau} \sum_{i=D_M}^{m} H_{ij}$ instead of Eq. (14). (**D**) As per (C) but in logarithmic frequency scale.

where q_M and q_T are the entropic indices for the magnitude and interevent times respectively and Δt_0, is the *q-relaxation time*, analogous to the relaxation (characteristic) time often encountered in the analysis of physical systems. On taking the logarithm and setting $a = \log(N_0)$ Eq. (16) becomes

$$\log N\left(>\{M \geq M_{th},\ \Delta t : M \geq M_{th}\}\right) =$$
$$= a \quad + \quad \left(\frac{2-q_M}{1-q_M}\right) \cdot \log\left(1 - \frac{1-q_M}{2-q_M} \cdot \frac{10^M}{\alpha^{2/3}}\right) \quad + \quad \frac{1}{1-q_T} \log\left(1 - \Delta t_0^{-1}(1-q_T)\Delta t\right) \tag{17}$$

Eq. (17) is a generalized (bivariate) law of the Gutenberg – Richter kind in which

$$b_q = \frac{(2-q_M)}{(q_M - 1)} \tag{18}$$

is the NESP equivalent of the *b* value (also see Telesca, 2012). Accordingly, Eq. (17) is the general model to be implemented in the ensuing analysis. Notably, Eq. (17) has also been applied to the analysis of the time dependence of complexity along the San Andreas Fault (Efstathiou et al., 2015), as well as to a

preliminary study of the spatiotemporal properties of seismicity in South California (Efstathiou et al., 2016).

The logarithmic form of the distribution shown in Fig. 2b can be approximated with Eq. (17) using non-linear least-squares. Because the parameters of Eq. (17) are subject to positivity constraints and/or are bounded (e.g. the entropic indices), a solver implementing the *trust-region reflective* algorithm was chosen (e.g. Moré and Sorensen, 1983; Steihaug, 1983), together with *least absolute residual* (LAR) minimization so as to suppress possible outliers. A *typical* outcome of this procedure is shown in Fig. 3a. The quality of the approximation is exceptional, with the correlation coefficient (R^2) being as high as 0.99. The magnitude entropic index q_M = 1.51 so that $b_q \approx 1$, which compares very well to conventionally computed b values. The temporal entropic index q_T = 1.3 indicating weak non-extensivity. The evaluation of the result is summarized in Fig. 3b and is based on the analysis of the statistical distribution of the residuals (r_s). The observed cumulative probability of the sorted residuals is fitted with a normal location-scale distribution (dashed line) and a Student-t location-scale distribution (solid line). Evidently, 85% of the residual population, for which $|r_s| \leq 0.1$, is normally distributed. A very short truncated tail appears to form at $r_s < -0.1$; it comprises 39 residuals or approx. 16% of the population and does not deviate significantly from normality. A long tail forms at $r_s > 0.2$, which is not successfully fitted with either the

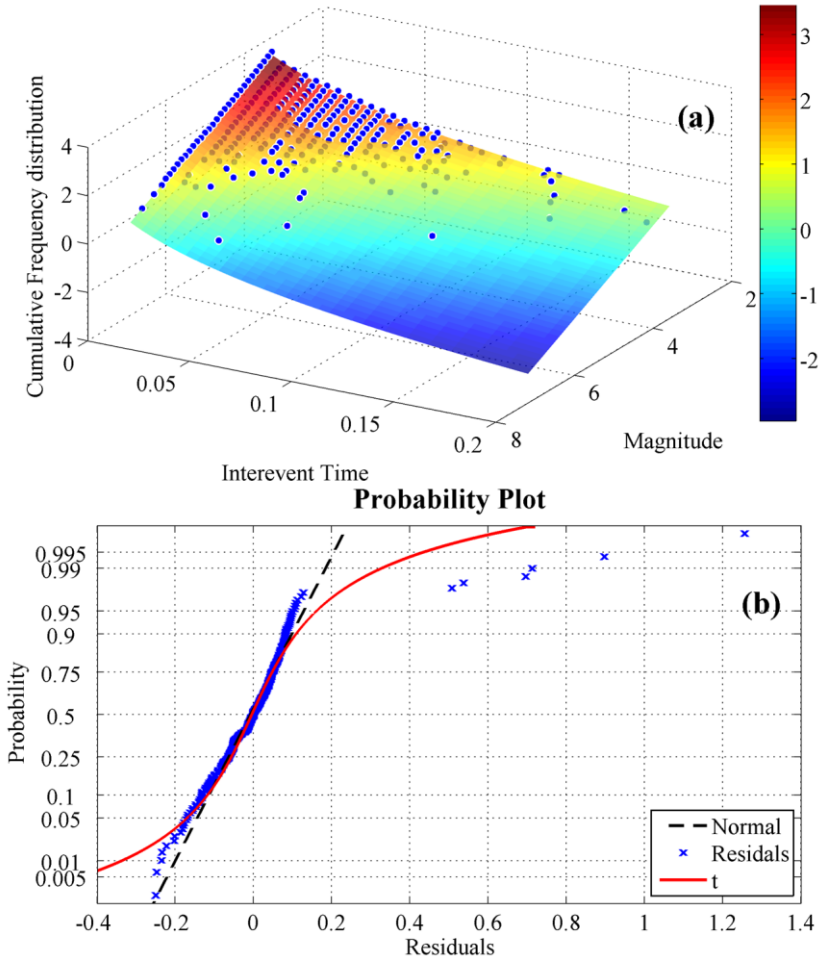

Figure 3. (a) The logarithmic frequency scale F-M-T distribution of Fig. 2b together with the model fitted using Eq. (17). **(b)** Probability analysis of the residuals (see Section 2.2.1 for details).

normal or the *t*-location-scale distribution. This comprises only 7 out of 244 residuals (2.87%) and represents *outliers* that have been effectively suppressed by the LAR procedure: the solution is determined by the remaining 97.13% of the observations.

The outliers mainly occur at larger magnitudes and longer interevent times. They may be glitches of the catalogue, (e.g. missing events or sequences of events, errors in magnitude reporting etc.). Nevertheless, some may also be genuine exceptions to the underlying seismogenetic process: for instance, they may correspond to rare, externally driven events. Herein, we shall not delve into such details but it is interesting to point them out. It is also significant to note that according to Eq. (14), the cumulative distribution is formed by stacking only the populated (non-zero) bins of the incremental distribution. This constraint has been introduced *because* of the outliers! Without the constraint, the unpopulated bins backwards of the outliers would have been included in the summation. This would have resulted in an awkward stepwise "distribution" in which the *unpopulated* bins (unknown probability densities) lying between the outliers and the populated bins would appear as patches of equal frequency (uniform probability), exactly as shown in Fig. 2c and 2d. This, in turn, would imply that the high probability zones of the observed bivariate distribution would comply with certain, well specified laws, but the lower probability zones would, somehow, include uniform stretches. In one-dimensional distributions this effect may not stand out, or significantly influence parameters estimation, and is often neglected. In multivariate distributions however, in addition to the obvious absurdity, it would be numerically detrimental.

To conclude this section, we note that in order to distinguish between proximal and distal earthquakes and evaluate their correlation, we apply the above modelling procedure to subsets of the catalogue in which earthquakes are grouped by interevent distance according to the rule

$$C \supset \{C_D : M > M_{th} \wedge \Delta d_L \leq \Delta d \leq \Delta d_U\} \tag{19}$$

where C is the catalogue, C_D is the subset catalogue, Δd is the interevent distance and Δd_L, Δd_U are the upper and lower group limits. This, is tantamount to constructing and modelling the conditional bivariate cumulative distribution

$$P\big(> \{M \geq M_{th},\, \Delta t : [M \geq M_{th} \wedge \Delta d_L \leq \Delta d \leq \Delta d_U\,]\}\big) \tag{20}$$

as a proxy of a trivariate F-M-T-D distribution.

3. Earthquake data

The present study focuses on the seismicity of North California, USA, partly due to its reliable earthquake monitoring services and seismological catalogues and partly because Californian seismicity is a test bed for the development of seismogenetic models, therefore an appropriate place to conduct this type of research. The study area is bounded by the coordinates 34°N to 41°N and -126.0°E to -116.0°E and includes different earthquake source areas, as can be seen in the composite seismicity map of Fig 4. These are:

(a) The broader area of the central and northern segments of the San Andreas Fault, (henceforth nSAF), where earthquake epicentres are indicated with white rectangles. This is a well-known, highly active fault system and has generated large (M > 7) earthquakes during the last two centuries (e.g. 1857, 1906, 1989). It extends northward of the Garlock Fault (see below), between Parkfield at approximately (35.9°N, 120.4°W) and the Mendocino Triple Junction (approx. 40.36°N, 124.6°W). For the purpose of this study, the geographic boundaries of nSAF are defined to the north by the line joining the northern terminus of the SAF/Shelter Cove section (40.2°N, -124.3°E), the northern terminus of the Barlett Springs Fault System (Lake Mountain fault) and the Battle Creek Fault

(40.5°N, -121.9°E); to the east by the Battle Creek Fault, the Foothills Fault system (roughly through 39.3°N, -118.8°E) and the Kern Gorge and White Wolf fault zones (roughly 35.3°N, -118.6°E); to the south by the Garlock Fault, roughly between (35.1°N, -117.3°E) and (34.6°N, -120.5°E), at the western terminus of the Santa Ynez Fault Zone – Pacific Section which is a virtual extension of the Garlock fault; to the west by an imaginary line running offshore parallel to the Pacific Coast.

(b) The Central Valley – Sierra Nevada Range, up to and including the Walker Lane to the east, where epicentres are indicated with solid black circles (henceforth SNR); this fault system also extends northward of the Garlock Fault and behaves as a semi-rigid microplate (Sierran microplate) whose interior (Central Valley) is often described as rigid and is characterized by the absence of significant faults and large earthquakes (Hammond et al, 2012; Saleeby et al., 2009; McCaffrey 2005; Dixon et al., 2000; Goter et al., 1994). In this study the geographic boundaries of SNR are defined to the north by the line joining the Battle Creek Fault and the northern termini of the Butt Creek and Almanor fault zones (approx. 44.5°N, -121.2°E), up to the longitude -116°E; to the east by the meridian -116°E; to the south by the Garlock Fault, approx. between (35.6°W, -116.3°E) and (35.1°N, -117.3°E); to the west by the White Wolf and Kern Gorge fault zones, the Foothills Fault system and the Battle Creek Fault.

(c) The Mendocino Fracture Zone (MFZ) and Triple Junction where epicentres are indicated with light grey down triangles.

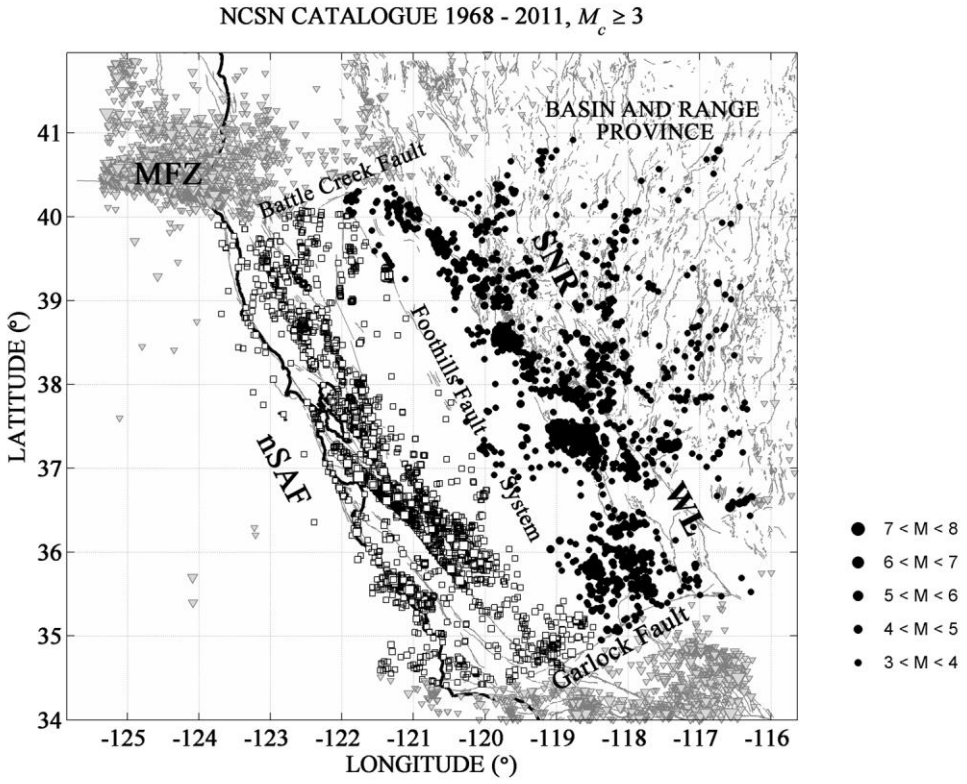

Figure 4a. The seismicity of North California as illustrated by mapping the epicentres of earthquakes included in the full NCSN catalogue for the period 1968-2011. nSAF represents the north segment of the San Andreas Fault with earthquake epicentres depicted as white rectangles. SNR-WL represents the Sierra Nevada Range – Walker Lane system with earthquake epicentres depicted as solid black circles. The epicentres of earthquakes *not* included in the ensuing analysis (e.g. Mendocino Fault Zone – MFZ) are depicted as light grey down-pointing triangles.

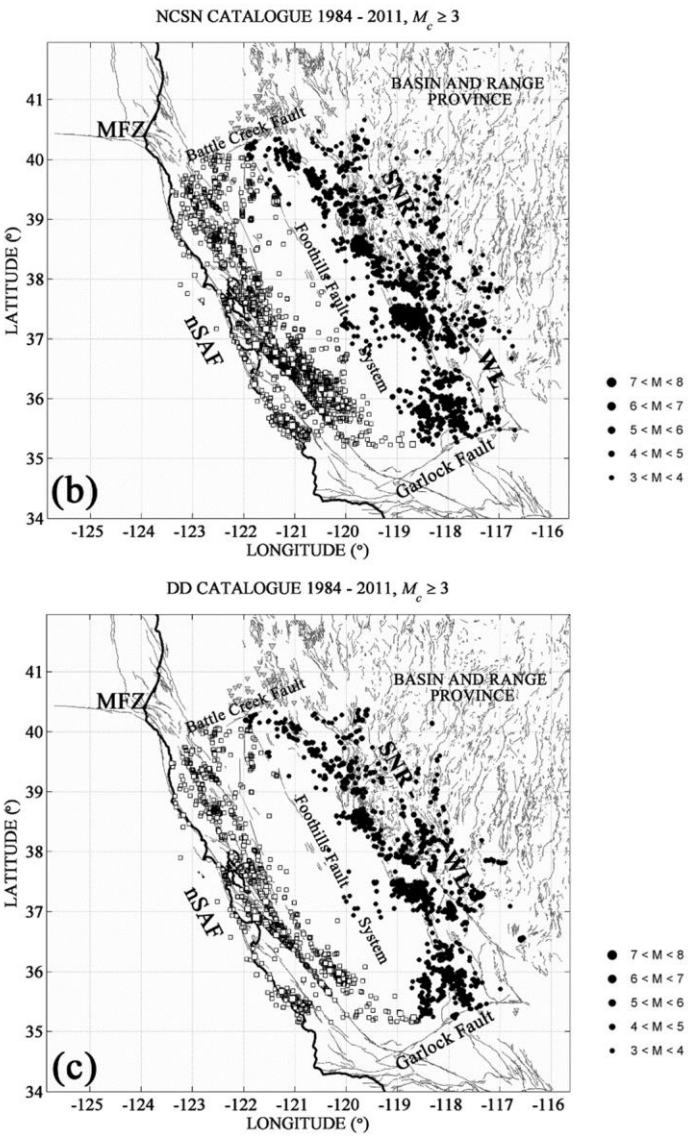

Figure 4b, c. Comparative epicentre distribution of **(a)** the full NCSN and **(b)** the full DD catalogues, for the same period (1984-2011), geographical boundaries and magnitude of completeness ($M_c \geq 3$). As per Fig. 4a, the nSAF epicentres are illustrated as white rectangles and the SNR epicentres as solid black circles.

The southern margin of the study area is taken to be northward of the ENE-WSW oriented, left-lateral Garlock Fault Zone (GFZ). This is a major boundary between the Great Basin (extending to the east of Walker Lane), and the Mojave Desert extending to the south and southwest; it is characterized by a mixture of left-lateral strike-slip and reverse focal mechanisms and is believed to have developed in order to accommodate the strain differential between the dominantly extensional tectonics of the semi-rigid Great Basin microplate and the right lateral strike-slip faulting of the Mojave Desert's crust. The intersection of the Garlock and San Andreas faults begets a restraining bend located approx. between 34.5°N and 35.5°N (Big Bend), where the strike of the SAF and the mode of deformation are notably different from that experienced in either side of the bend (e.g. Jones, 1988; Hardebeck and Hauksson, 2001). Studies based on slip rates, focal mechanisms etc. indicate that the GFZ is the area where the SAF and the East California Shear Zone lock up in Southern California and a tectonic boundary forms between

north and south California, delimiting the central/north and south segments of the SAF (e.g. Fialko, 2006; Becker et al, 2005). The Mendocino Fracture Zone includes the seismically most active expanse of North California (Yeats, 2013); according to Dengler et al. (1995), the north coastal region accounted for about 25% of the seismic energy released in California in a 50 year period. However, the MFZ is not included in the present analysis as we consider that it must be studied separately: it is a significant feature whose geodynamic characteristics clearly distinguish it from the nSAF and SNR. Accordingly, the source areas to be considered in the present analysis are the nSAF and the SNR as shown in Fig. 4, which are both characterized by NW-SE, dominantly right-lateral strike slip deformation due to pure transformational and transformational to trans-tensional stress regimes respectively.

The recent earthquake history of North California is summarized in two definitive catalogues published by the North California Earthquake Data Center (NCEDC, http://www.ncedc.org):

a) The original NCEDC catalogue, henceforth to be referred to as the *NCSN catalogue* (for Northern California Seismic Network). Therein, most earthquake sizes are reported in the local (M_L) and moment (M_w) magnitude scales but a considerable number of events is reported in the duration (M_d) and amplitude (M_x) scales. The latter have been exhaustively calibrated against the M_L scale: Eaton (1992) has shown that they are within 5% of the M_L scale for magnitudes in the range 0.5 to 5.5 and that they are virtually independent of the distance from the epicentre to at least 800 km. In consequence, M_d and M_x are practically equivalent to M_L. For the purpose of the present analysis M_w magnitudes were also converted to M_L using the empirical formula of Uhrhammer et al (1996): $M_w = M_L \cdot (0.997 \pm 0.020) - (0.050 \pm 0.131)$. Herein we will use a subset of this catalogue spanning the

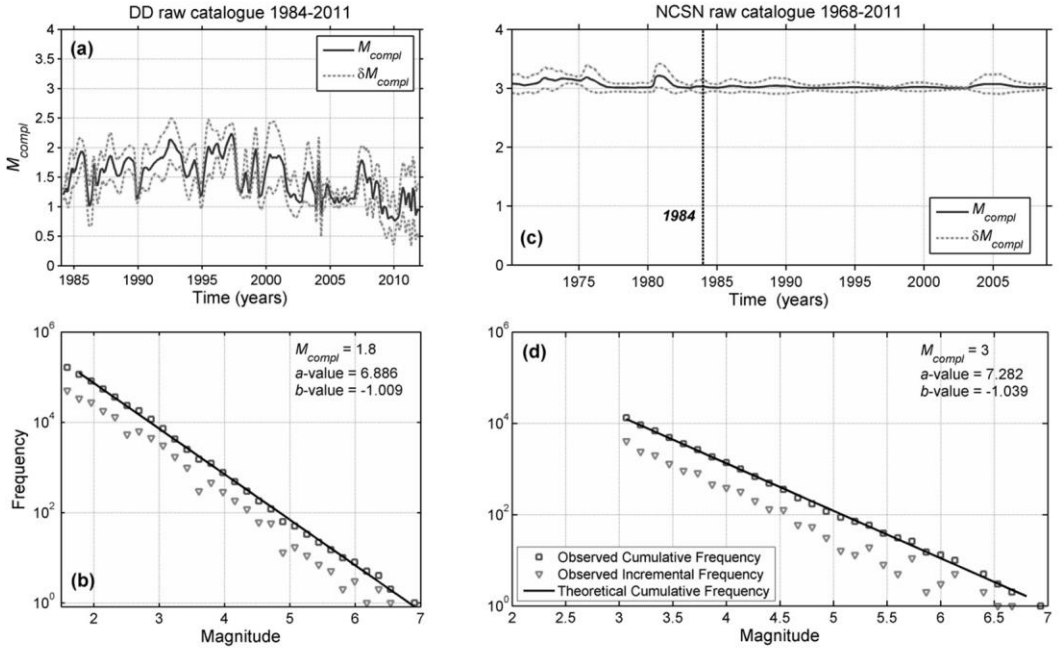

Figure 5. a) Variation of the magnitude of completeness (M_{compl}) with time in the DD catalogue with 95% confidence limits. **b)** Incremental (down triangles) and cumulative (open squares) F-M distributions of the DD catalogue above the magnitude of completeness. **c)** Variation of M_{compl} with time in the NCSN catalogue with 95% confidence limits. **d)** Incremental (down triangles) and cumulative (open squares) F-M distribution of the NCSN catalogue above the magnitude of completeness. Figs. 5a and 5c were prepared with the *ZMAP* software (Wiemer, 2001).

period 1968–2012 which, after homogenization of the magnitude scale was found to be complete for $M \geq 3.0$ (Fig. 5c and 5d). The epicentre distribution of this subset is shown in Fig. 4a.

b) An updated/upgraded version of the NCEDC catalogue in which waveform cross correlation and double-difference methods were used to improve the hypocentral locations of earthquakes observed during the period 1984–2011, by up to three orders of magnitude (Waldhauser and Schaff, 2008; Schaff and Waldhauser, 2005). This is will be dubbed the *Double Difference* (DD) catalogue by reference to the relocation method. Therein, earthquakes locations are reported only for latitudes northward of 35.3°N and earthquake sizes are reported in the local magnitude scale; the catalogue is complete for $M \geq 1.8$ and for the entire period 1984-2011 (Fig. 5a, 5b) and the epicentre distribution is shown in Fig. 4c.

There are *significant* differences in the information contained in the two catalogues: when constrained by the same geographical boundaries (as per Fig. 4b and Fig. 4c), time interval (1984–2011) and magnitude of completeness ($M_c \geq 3.0$), the NCSN catalogue was found to comprise 6696 events and the DD catalogue 7465. However, the difference is *not* limited to 769 events as would appear at first sight: not

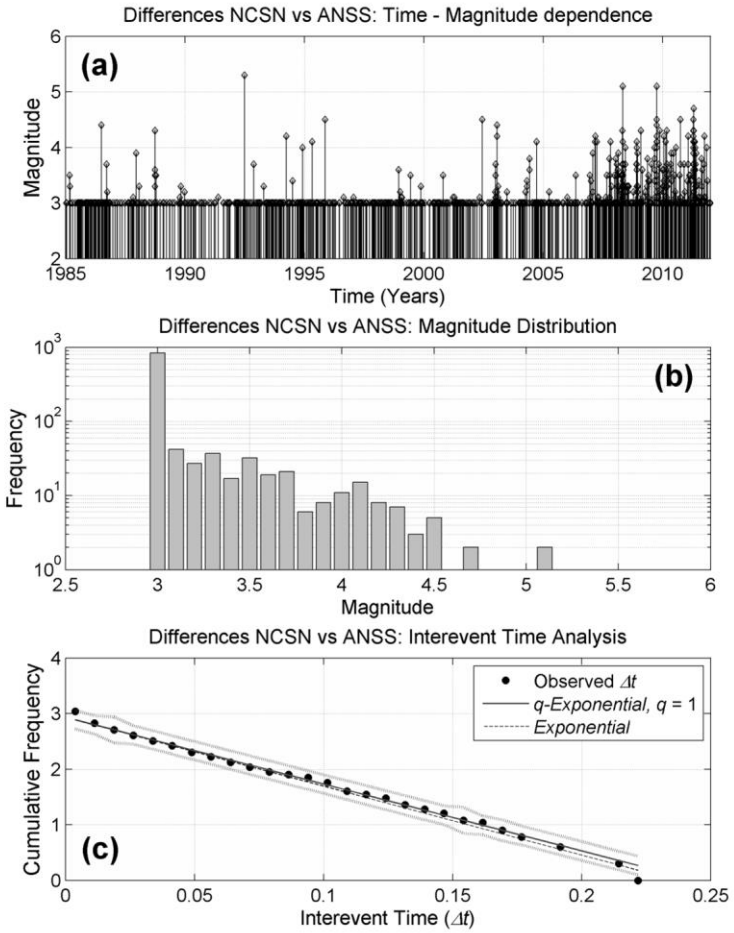

Figure 6. (a) Time-Magnitude diagram of the differences between the NCSN and DD catalogues. **(b)** Incremental frequency–magnitude distribution of the events shown in (a). **(c)** Black solid circles represent the empirical cumulative frequency – interevent time distribution of the events shown in (a); the distribution is almost perfectly fitted with a q-exponential function with $q \equiv 1$ (solid line), or with a conventional exponential function (dashed line).

only earthquakes present in the DD are missing from the NCSN catalogue, but also events present in the NCSN are missing from the DD! As evident in Fig. 6a**,** the missing events are generally interspersed with higher numbers of discrepancies clustering around larger earthquakes (main shocks) and exhibiting a very notable increase after year 2006. Thus, the total number of different event rises to an astounding 1102! As can also be seen in Fig. 6b, the number of discrepancies is overwhelming at the smaller magnitude scales, with a total of 839 differences at $M = 3$ and 1101 difference at $M \leq 4.6$. Even more interesting is that intermediate magnitude scales have also been affected. The sequence of missing events is completely random and unstructured: in Fig. 6c we demonstrate that the cumulative interevent time distribution can be almost perfectly modelled by a q- exponential function with $q \equiv 1$, or by a conventional exponential function. Finally, Fig. 6d is a map view of the differences between the NCSN and DD catalogues, in which the solid black circles illustrate the epicentres of earthquakes present in the DD but missing from the NCSN and white circles the same for earthquakes present in the NCSN but missing from the DD. It is clear that there is no obvious spatial pattern/ clustering of the differences and appear to be randomly distributed.

The discrepancy between the two catalogues can be explained as collateral of the relocation/ magnitude re-compilation process. According to Waldhauser and Schaff (2008) some events are "re-evaluated" and some may even be lost because of insufficient data links after the weighting function removes outliers. The analysis presented in Fig. 6 seems to indicate that the "re-evaluation" has migrated a significant number of events with original (NCSN) magnitudes lower than 3 to eventual (DD) magnitudes ≥ 3 and a small number of events in the opposite direction, so that the DD has ended up richer in magnitude 3

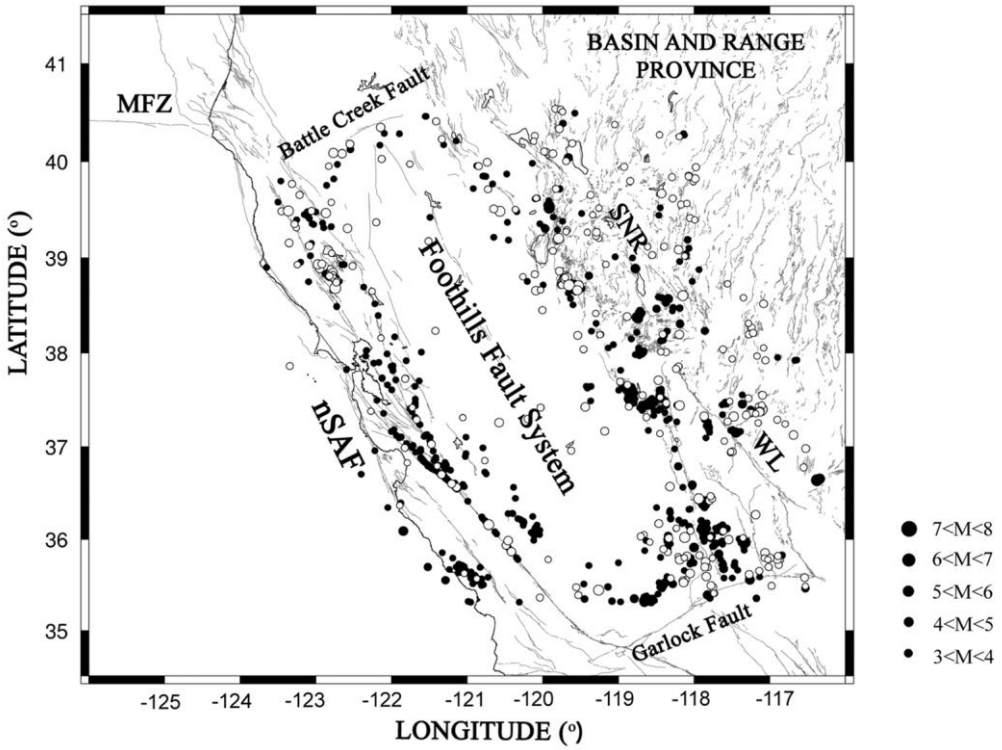

Figure 6d. Epicentre map of the differences between the NCSN and DD earthquake catalogues for the period 1984 - 2011. Solid black circles represent earthquakes present in the DD catalogue but *missing* from the NCSN catalogue. White circles represent earthquakes present in the NCSN catalogue but missing from the DD catalogue. No discernible spatial structure or clustering of the differences can be observed.

events with respect to the NCSN. Moreover, it appears to have done so in a rather unsystematic (random) way with respect to the temporal sequence of events. It should also be pointed out that although this explanation would appear to be straightforward for discrepancies around the magnitude of completeness (M_c = 3), it does not answer the question of discrepancies observed at larger magnitude scales, the origin of which remains to us uncertain (especially after 2006).

The effect of unsystematic surplus or deficit of events in a catalogue may be significant: it not only produces outliers as mentioned above (Section 2.2.1), but is also expected to distort and possibly randomize the statistics of interevent time and interevent distance. It is therefore imperative to examine the extent to which such anomalies influence the declustering process and the estimation of the entropic indices. In seeking to conduct a thorough and rigorous as possible study, in Section 4 (Results) we shall first perform a comparative analysis of the NCSN and DD catalogues for events observed within identical geographical boundaries during their common interval 1984–2011 and for magnitudes equal to, or greater than a threshold of M_{th} = 3.0. The results of this exercise will expectably indicate the more consistent catalogue, on the basis of which to evaluate the statistical mechanics of North California seismicity.

3.1. Declustering

As stated in the introduction, it is not clear whether the background seismogenetic process is fundamentally random or correlated; moreover there has been a vigorous debate as to whether the power laws implied by the empirical F–T distributions are characteristic and universal, or only a result of mixing correlated foreground and uncorrelated background processes. In order to address these questions it is important to conduct the analysis on declustered versions of the earthquake catalogues, in which the aftershock sequences have been eliminated in an optimal as possible way.

Herein we implement the stochastic declustering method of Zhuang et al. (2002), the principal reason being that it is built on the premise of self-excited Poisson processes: if background seismicity obeys Boltzman-Gibbs statistics, then it should be able to extract a nearly random background process against which to test alternative hypotheses. The method is based on space-time branching approaches to describe how each event triggers its successors. The choice of the space-time distance is optimized by fitting an ETAS model to the earthquake data and there is no need to assume anything about the parameters pertaining to the definition of the space-time distance (although a parametric form of said distance is assumed a priori). In addition, instead of associating an aftershock to only one main shock, the method assigns each earthquake with a probability to be an aftershock of a preceding earthquake. This means that all preceding earthquakes are possible main shocks of the events that follow them and is advantageous in that it circumnavigates the difficulty of making committing binary decisions in the very frequent case of nearly equal space-time distances between successive events.

The Zhuang et al. method uses the following form of the normalized probability that one event will occur in the next instant, conditional on the hitherto history of the seismogenetic process (conditional intensity):

$$\lambda\left(t,x,y,M \mid H_t\right) = \mu\left(x,y,M\right) + \sum_{i:t_i<t} \kappa\left(M_i\right)\cdot g\left(t-t_i\right)\cdot f\left(x-x_i, y-y_i \mid M_i\right)\cdot j(M \mid M_i)$$

where, λ is the conditional intensity on the history of observation H_t until time t, $\mu(x, y, M)$ is the background intensity, $\kappa(M)$ is the expected number of foreground events triggered by a magnitude M main shock and $g(t)$, $f(x,y|M_i)$ and $j(M|M_i)$ are respectively the probability distributions of the occurrence time, the location and the magnitude events triggered by a main shock of magnitude M_i. If the

catalogue is arranged in chronological order, then the probability of an event j to have been triggered by an event $i < j$ can be estimated from the occurrence rate at its occurrence time and location as

$$p_{i,j} = \frac{\kappa(M_i) \cdot g(t_j - t_i) \cdot f(x_j - x_i, y_j - y_i \mid M_i)}{\lambda(t_j, x_j, y_j \mid H_t)}$$

and the probability that an event j is aftershock is given by

$$p_j = \sum_{i=1}^{j-1} p_{i,j}$$

Conversely, the probability that an event j is background is given by

$$\phi_j = 1 - p_j = \frac{\mu(x_j, y_j \mid H_t)}{\lambda(t_j, x_j, y_j \mid H_t)}$$

The algorithm runs iteratively through the catalogue and by assigning probabilities $p_{i,j}$, p_j and ϕ_j to the j^{th} event generates the foreground sub-process associated with the i^{th} event (i.e. its aftershock sequence). It thus separates the catalogue into a number of sub-processes whose initiating events comprise the background. As a general rule, events with $\phi_j \leq 50\%$ are considered to be foreground.

Since the output of stochastic declustering is not unique, it is useful to use the probabilities $p_{i,j}$ and ϕ_j to generate different realizations of the declustered catalogue at different probability levels and use them to test hypotheses associated with background seismicity and/or aftershock clustering. Our analysis herein will be based on the assumption that events with probability $\phi_j \geq 70\%$ are likely to be background. Fig. 7a illustrates the cumulative earthquake count of the full NCSN catalogue for the period 1968-2012 (thick black line) and its declustered versions with probability $\phi_j \geq 70\%$ (thin black line), $\phi_j \geq 80\%$ (solid grey line) and $\phi_j \geq 90\%$ (dashed grey line). The catalogue declustered at the $\phi_j \geq 70\%$ level is almost free of the time-local rate surges (jerks) that indicate the presence of aftershock sequences. Nevertheless, it is not completely smooth and exhibits small fluctuations because a portion of the remaining events are

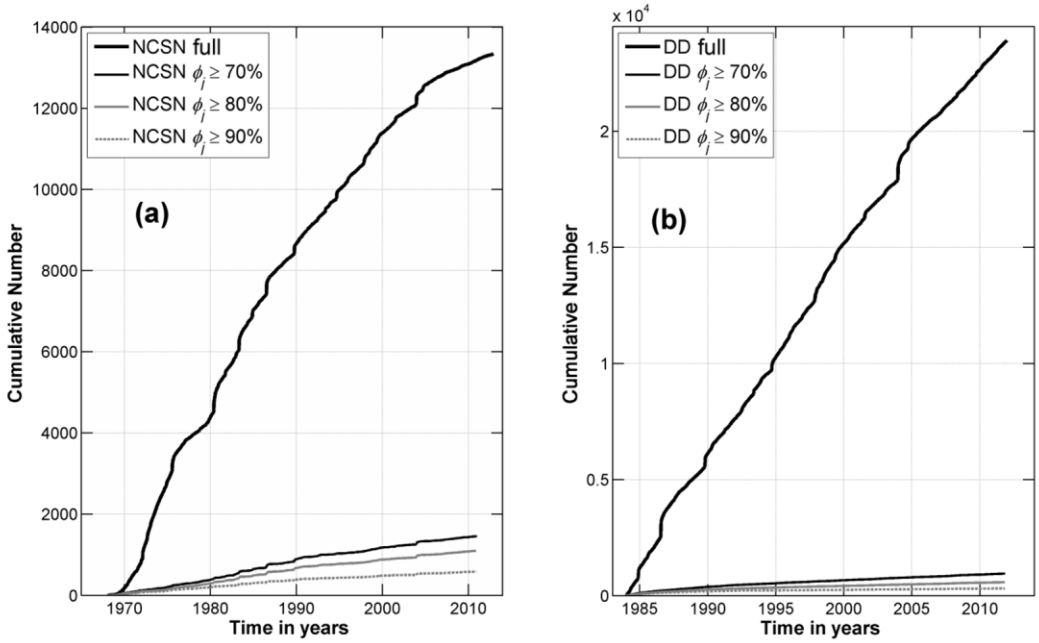

Figure 7. a) The cumulative earthquake count of the observed (full) and declustered realizations of the NCSN catalogue. **b)** The cumulative earthquake count of the full and declustered realizations of the DD catalogue.

foreground residuals. Consequently, in dealing with the NCSN catalogue, we will endeavour to confirm the results obtained at the 70% probability level by studying declustered realizations with probability $\phi_j \geq$ 80% and $\phi_j \geq 90\%$ to be background. Fig. 7b illustrates the corresponding cumulative count of DD catalogue realizations as per Fig 7a: the thick black line corresponds to the full catalogue and the thin black, solid grey and dashed grey lines to realizations declustered at $\phi_j \geq 70\%$, $\phi_j \geq 80\%$ and $\phi_j \geq 90\%$ respectively. Clearly, the full DD catalogue contains more events than the full NCSN but its declustered realizations contain significantly fewer events than the corresponding realizations of the NCSN. This we explain as collateral of relocation: epicentres and hypocentres become compactly spaced so that the space-time distance between consecutive events decreases and their likelihood of being classified in the foreground increases. The cumulative count of the DD catalogue declustered at the $\phi_j \geq 70\%$ level is very smooth. In addition, the number of events at this level is not significantly different from the number of events remaining at higher probability levels. This indicates that to all intents and purposes, the $\phi_j \geq 70\%$ catalogue is free of foreground events.

4. Results

4.1. Determination of randomness thresholds

Complexity and self-organization are associated with long-range interactions and long-term memory; these properties are collectively referred to as "correlation". NESP theory proposes that the entropic indices are measures of such correlation: when $q \neq 1$, the system is non- extensive; when $q \to 1$ the system should be random, uncorrelated and memoryless. Accordingly, if the seismogenetic process is non-extensive q_T should differ from unity, thus expressing the interdependence of successive events in the correlated space-time of the seismogenetic system. However, b_q, as determined through q_M in Eq. (18), should be equivalent to the b value computed by conventional methods because the distribution of magnitudes does not relate the energies released by consecutive events, but only conveys information about the hierarchy of the active fault system. On the other hand, if the seismogenetic system is extensive one should obtain $q_T \to 1$ and the third term in the RHS of Eq. (17) should reduce to the logarithm of the exponential distribution, but b_q should still be equivalent to the b value computed by conventional methods. In both cases, the favourable comparison of b_q (that is q_M) to the results of well-established methods of b-value estimation should be a rather robust means of ensuring the validity of the numerical procedure used in approximating Eq. (18) and the robustness of the results and conclusions.

In order to determine a threshold value of the temporal entropic index q_T, above which it is safe to assume non-Poisson seismogenetic processes, we analyse many synthetic background catalogues constructed on the basis of the ETAS model, which should yield temporal entropic indices with an expectation of unity. In this study, we implement the stochastic ETAS aftershock simulator program "AFTsimulator" by Felzer (2007). The program uses empirical statistical laws of background and aftershock behaviour (i.e Omori law, Gutenberg-Richter law), and Monte Carlo methods to simulate background earthquakes and multiple generations of aftershocks. Known main shocks are input as point or planar sources and background earthquakes are chosen randomly from observed or contrived spatial distributions (grids) of earthquake rates. This facilitates the generation of realistic synthetic background catalogues, absolutely consistent with the known long-term seismotectonic characteristics of a given region (for a detailed theoretical background see Felzer et al., 2002 and Felzer and Brodsky, 2006). In our implementation of the AFTsimulator we have used the ETAS parameterization obtained (fitted) by declustering the NCSN catalogue, assumed a uniform background seismicity rate such that b = 1 and have set the maximum

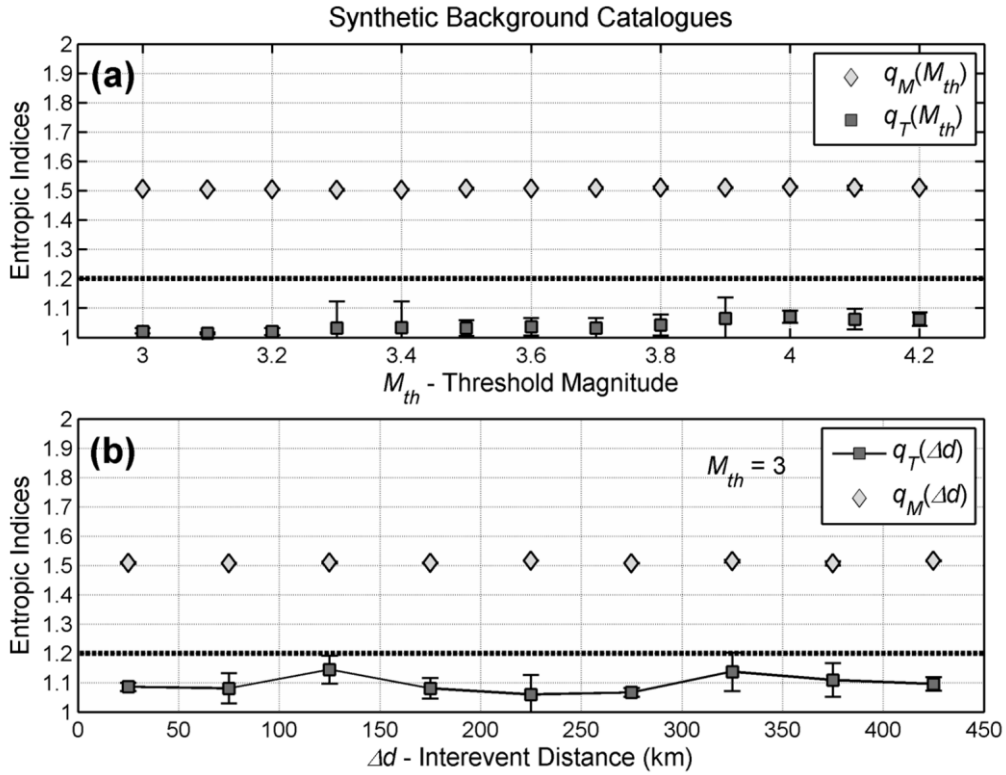

Figure 8. NESP analysis of 20 synthetic ETAS background catalogues constructed with the characteristics of North Californian seismicity and spanning a period of 44 years. **(a)** Mean values $\bar{q}_M(M_{th})$ and $\bar{q}_T(M_{th})$ of the entropic indices and associated 3σ error margins, computed for different threshold magnitudes (M_{th}). **(b)** Mean values $\bar{q}_M(\Delta d)$ and $\bar{q}_T(\Delta d)$ of the entropic indices and associated 3σ error margins computed for different interevent distance groups (Δd). In both cases, the horizontal dashed line at q = 1.2 indicates the threshold above which the temporal entropic index q_T can be *safely* assumed to indicate non-Poissonian processes.

expected magnitude to be M_L = 7.2, the same as the maximum observed over the 44-year period 1968-2012 (the Loma Prieta earthquake of 1989).

Fig. 8 illustrates the NESP analysis of 20 synthetic background catalogues, each spanning a consecutive 44 years. Fig. 8a illustrates the variation of the mean values $\bar{q}_T$ and $\bar{q}_M$ computed from the analysis of all synthetic catalogues and associated 3σ error margins, as a function of the threshold (cut-off) magnitudes M_{th}. It is apparent that all $\bar{q}_T(M_{th})$ are consistently lower than 1.1, indicating very low correlation – effectively randomness – without exception. Likewise, all $\bar{q}_M(M_{th})$ exhibit an almost imperceptible variation around 1.5, so that $b_q \approx 1$, consistently with the assumptions on which the synthetic ETAS catalogues were constructed and the observed *b*-values of the NCSN and DD catalogues (see Fig. 5). It is also apparent that the populations $\{q_T(M_{th})\}$ and $\{q_M(M_{th})\}$ from which $\bar{q}_T(M_{th})$ and $\bar{q}_M(M_{th})$ have been derived are remarkably consistent: the 3σ error level is generally very small and, in most cases, the 3σ error bars its smaller than the size of the symbols representing the expectation values! Fig. 8b illustrates the variation of entropic indices computed by grouping the earthquakes of the synthetic catalogues according to interevent distance (Eq. 19) and modelling the conditional probability function

expressed by Eq. (20). The breadth of the interevent distance groups (Δd) is indicated with horizontal bars. The results have been derived by considering all earthquakes above a magnitude threshold M_{th} = 3.0 and as above, the panel illustrates mean values $\bar{q}_T(\Delta d)$, $\bar{q}_M(\Delta d)$ together with their associated 3σ error margins. Again as above, all $\bar{q}_T(\Delta d)$ are consistently low for all interevent distance groups, so that max[$\bar{q}_T(\Delta d) + 3\sigma] \leq 1.2$, while $\bar{q}_M(\Delta d)$ are also very stable and exhibit small fluctuations around 1.5, so that $b_q \to 1$ as expected.

The above exercise was conducted with several truly random background catalogues generated on the basis of the ETAS model. In consequence, it can be concluded that the analytical procedure described in Sections 2.2 and 2.3 yields stable magnitude entropic indices and *proxy b-values* (b_q) compatible with *b*-values determined by conventional methods. More importantly, however, the results establish that the systematic observation of experimental q_T values greater than 1.2 would be compelling evidence of non-extensive seismogenetic dynamics.

Last but not least, we shall provide an answer to this hypothetical question: Since the synthetic ETAS catalogues contain events whose sequence is by construction random in time, why isn't q_T always arbitrarily close to unity, but may deviate by as much as 0.2? After all, Fig. 6c demonstrates that $q \approx 1$ in the case of truly Gaussian univariate sequences (which can be *equivalently* approximated with *q*-exponential and standard exponential functions). The answer is that the AFTsimulator draws random numbers from a *uniform* distribution. On the other hand, experimental realizations of q_T computed on the basis of Eq. (17) can be arbitrarily close to unity *only* for exponentially distributed interevent time data. When uniformly distributed data is used instead, the minima of the parameter space are *expected* to move away from unity by a small, albeit not always insignificant distance. In addition, given the local nature of least-squares solvers, this distance is expected to vary between different synthetic earthquake ensembles, thus generating the variability observed in Fig. 8. Conversely, the distribution of magnitudes in the synthetic catalogues is made to follow the Gutenberg-Richter law; as a result, q_M does not exhibit any variability whatsoever. Although we identified this issue early on, we chose not to adjust the original AFTsimulator code even if this meant that we had to "sacrifice" perfectly legitimate lower-valued temporal entropic indices. Given the intensity of the discourse between the Poissonian and non-Poissonian doctrines we made this decision because we felt that we had to establish a very rigorous criterion, and for that matter one that ensures that whatever inference we make will be trustworthy and hard to contend.

4.2. Analysis of Full Earthquake Catalogues

In order to conduct a comprehensive as possible study, our investigation will comprise a comparative analysis of the NCSN and DD catalogues over the (common) period 1984–2011, as well as detailed analysis of the NCSN catalogue for the extended period 1968 – 2011 (44 years). We will also conduct a detailed comparative study of seismicity in the nSAF and SNR areas over the period 1968 – 2011. Full and declustered catalogues will both be considered. The analysis will focus on the properties and variation of the entropic indices with respect to threshold magnitude, (M_{th}) and interevent distance (Δd). The results are summarized in Tables 1 and 2 and displayed in Figures 9 to 15. For the sake of experimental rigour, estimation of the entropic indices is *not* performed for data sets (sub-catalogues) containing *less than* 300 events and results are *not* considered and displayed *unless* associated with a goodness of fit (R^2) *better* than 0.97.

4.2.1 Comparative study of the full NCSN and DD catalogues (1984 – 2011)

As shown in Section 3, the NCSN and DD catalogues contain different information in the sense that events present in one catalogue are missing from the other and vice versa. The differences are randomly distributed in space and in time and their sizes cluster in the lower magnitude range, with 945 observed at $M_L \leq 3.3$ and 1101 $M_L \leq 4.6$. Overall, the DD catalogue contains 769 events more than the NCSN and we consider unlikely for the NCSN to have missed a hundreds of earthquakes at these magnitude scales. Rather, in Section 3 we have argued that the re-compilation process by which the DD catalogue was put together may have moved a significant number of events up the hierarchy and although the changes were definitely short-spanned, (original and eventual magnitudes were generally not far apart), it is easy to see how the natural hierarchy of earthquake sizes would inadvertently be tampered with: this we dub *hierarchical restructuring* of the catalogue. Now, consider that if correlations (complexity) indeed exist, and because earthquake frequency decreases with magnitude (Gutenberg-Richter law), this type of restructuring increases the probability of inserting at higher hierarchical echelons, events that are *not* correlated with the events naturally occupying those echelons. This, in turn, is likely to have a net of randomizing effect on the empirical F-M-T distribution, meaning that fat tail (power-law structure) of the true F-M-T distribution would thinned and pushed towards exponential. It is self-evident that the differences in information content necessitate a comparative study of the NCSN and DD catalogues, not only because it is pivotal in appraising the results obtained from either catalogue, but also because it is instrumental in appraising the performance of our estimation procedure and its sensitivity to (inadvertent or not) changes in the hierarchy of event sizes.

The results of the comparative analysis are illustrated in Fig. 9. As can be seen in Fig. 9a, $q_M(M_{th})$ determinations from both catalogues are very stable and practically identical, varying smoothly from 1.49 at $M_{th} = 3$ to 1.57 at the $M_{th} = 4.3$ and exhibiting steady, quasi-linear increase with increasing threshold magnitude. The application of Eq. (18) yields $b_q(M_{th})$ estimates that respectively vary from 1.04 to 0.75. The entropic index q_M, like the *b*-value to which it is related, represents the scaling of the size distribution of earthquakes and clearly indicates a correlated, scale-free process, possibly associated with a gradual change in the size distribution of active faulting. As can be seen in Table 1, the determinations of $b_q(M_{th})$ are consistent with the corresponding determinations of $b(M_{th})$ which have been computed with conventional (robust least squares) methods and vary in the interval 1.1 to 0.96. Turning our attention to the temporal entropic indices, we note that $q_T(M_{th})$ determinations from the NCSN catalogue (henceforth $q_T(M_{th})$-*NCSN*) are rather stable and for the most part vary between 1.2 and 1.3 so as to remain consistently above the "randomness threshold" of 1.2. Conversely, $q_T(M_{th})$ determinations from the DD catalogue (henceforth $q_T(M_{th})$-*DD*) are not as stable: for threshold magnitudes $M_{th} < 3.4$ they are consistently lower than 1.2 and differ from $q_T(M_{th})$-*NCSN* by more than 0.1, while for threshold magnitudes for $3.7 \leq M_{th} \leq 4.1$ they fluctuate erratically between 1.04 and 1.33.

As it turns out, the entropic indices exhibit two contrasting types of behaviour. The magnitude entropic index $q_M(M_{th})$ is very consistently determined for both catalogues. Conversely, the temporal entropic index $q_T(M_{th})$ exhibits differences with $q_T(M_{th})$-*NCSN* determinations being markedly and consistently stable in comparison to $q_T(M_{th})$-*DD*. We believe that we can offer a plausible exegesis of this effect, based on the inadvertent "restructuring" of earthquake size hierarchy in the DD catalogue. To begin with, it is likely that due to the nature of the integrand and the smoothing effect of integration, short-span changes in the hierarchy of event sizes will *not* stand out when forming univariate F-M distributions, or the F-M components of bivariate F-M-T distributions. In implementations of the DD catalogue in which univariate F-M distributions are normally used, any changes in the true values of the Gutenberg-Richter parameters *a* and *b* will expectedly be small and likely hidden in the estimation uncertainty. On the contrary, when

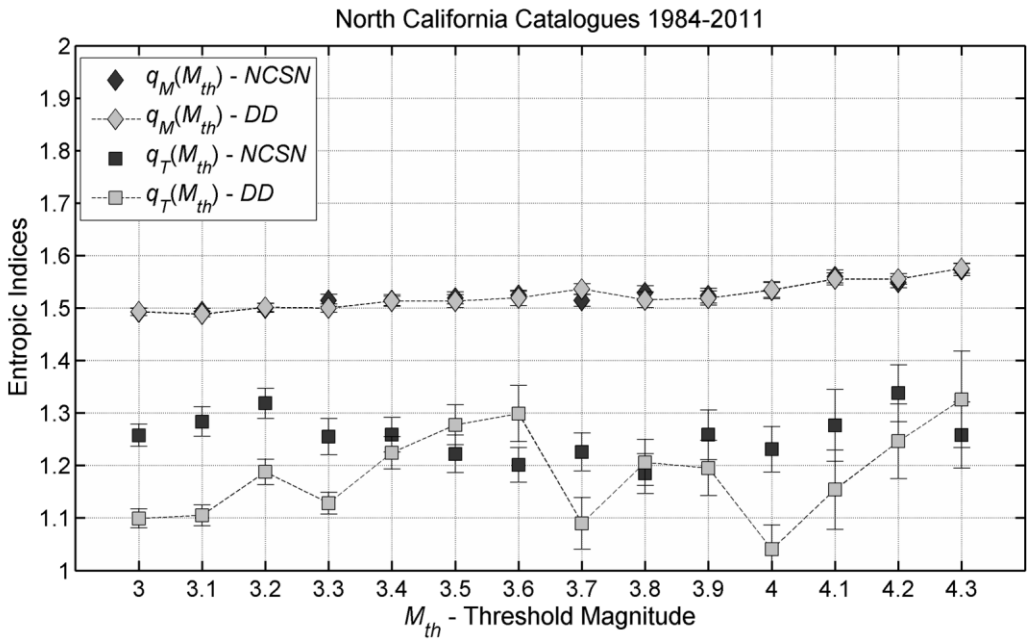

Figure 9a. Comparative analysis of the full NCSN and DD catalogues for the dependence of entropic indices on threshold magnitude (M_{th}). Dark grey symbols represent estimates based on the NCSN catalogue and light grey symbols estimates based on the DD catalogue. Error bars represent 95% confidence intervals. Comparisons are made for the period 1984-2011.

implementing the DD catalogue in ways sensitive to the manner by which information was altered, as for instance when forming frequency distributions of *differential quantities* such as interevent times and distances, distortions would likely not be as easy to suppress. Accordingly, we propose that the "restructuring" of the DD catalogue had a small effect on the stability of the F-M component of the empirical F-M-T distribution and resulted in consistent determinations of $q_M(M_{th})$-*NCSN* and $q_M(M_{th})$-*DD*, while it had an adverse randomizing effect on the F-T component of the F-M-T distribution and resulted in "inconsistent" determinations of $q_T(M_{th})$-*NCSN* and $q_T(M_{th})$-*DD*. The effect was expectedly pronounced at threshold magnitudes $M_{th} \leq 3.3$, where the bulk of the restructuring has apparently taken place and was also apparently destabilizing at thresholds $3.7 \leq M_{th} \leq 4.1$, where significant restructuring seems to have also taken place. Conversely, the rather stable determination of $q_T(M_{th})$-*NCSN* indicates that the NCSN catalogue is internally consistent with respect to the hierarchy of event sizes. Although an unknown number of events is certain to be missing at magnitudes near the threshold of $M_L = 3$, it appear that this is rather limited and randomly distributed in space and time, so as not to have any acute destabilizing effect.

Given all the above, it is also necessary to point out that both catalogues generally yield $1.1 < q_T < 1.3$ and discrepancies average to 0.07, so that $\bar{q}_T$ -*NCSN* = 1.26± 0.04 and $\bar{q}_T$ -*DD* = 1.18 ± 0.09 (Table 1). From this point of view the results can be deemed reasonably compatible, with NCSN providing evidence of marginally correlated and DD evidence of marginally uncorrelated seismogenetic processes.

The variation of entropic indices with interevent distance is shown in Fig. 9b. As before, the magnitude entropic indices $q_M(\Delta d)$ obtained from both catalogues are absolutely comparable with $\bar{q}_M$ (Δd)-*NCSN* = 1.5 ± 0.013 and $\bar{q}_M$ (Δd)-*DD* = 1.49 ± 0.016 (Table 2). The temporal entropic distances $q_T(\Delta d)$ are also very comparable for all interevent distances: for Δd up to 0-50km, $q_T(\Delta d)$ is 1.57 for the NCSN and 1.47 for the DD: these values indicate high correlation due to the overwhelming effect of near field interactions

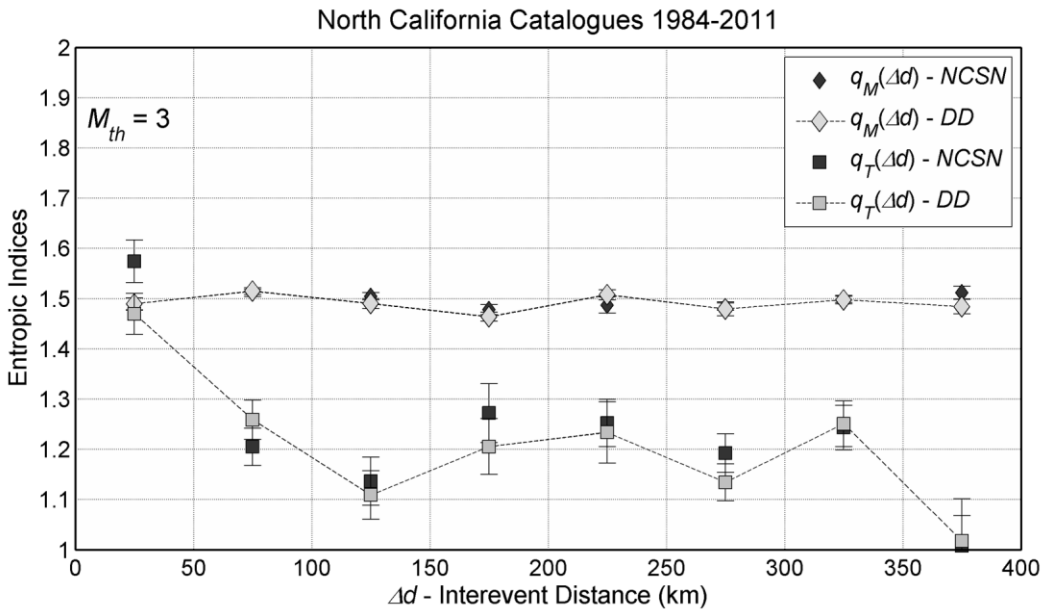

Figure 9b. Comparative analysis of the full NCSN and DD cataloguesfor the dependence of entropic indices on interevent distance (Δd). Earthquakes are binned according to Eq. (19) so that each bin spans a constant 50km; symbols are plotted at the midpoint of each bin. Dark grey symbols represent estimates based on the NCSN catalogue and light grey symbols estimates based on the DD catalogue. Error bars represent 95% confidence intervals. Comparisons are made for the period 1984-2011.

which are dominated by aftershock sequences. Conversely, for interevent distances longer than 100km, $q_T(\Delta d)$ drops to under 1.3 and fluctuates between 1.1 and 1.27 for Δd up to 350km, with mean values of 1.22 ± 0.05 for $q_T(\Delta d)$-*NCSN* and 1.20± 0.63 for $q_T(\Delta d)$-*DD*. It is rather remarkable that in spite of the differences in their information content, and albeit $q_T(\Delta d)$-*DD* is generally lower than $q_T(\Delta d)$-*NCSN*, the variation of the temporal entropic index q_T with interevent distance is rather similar for *both* catalogues. This we interpret to be a consequence of the fact that the "restructuring" of the DD catalogue is rather evenly spread across the study area as seen in Fig. 6d, so as to have a correspondingly less pronounced effect on F-M-T distributions formed by filtering earthquakes according to interevent distance. Both catalogues appear to indicate the presence of a weak long-range effect underlying the temporal expression of earthquake occurrence which, in turn, is taken to imply non-Poissonian dynamics.

Overall, the analysis of the temporal entropic indices points toward a weakly correlated seismogenetic system verging on the limit of randomness, at least during the period 1984-2011. Moreover, a) because the results obtained from the NCSN and DD catalogues are "reasonably compatible" and, b) because of our documented concern as to the consistency of the DD catalogue, we shall focus the rest of our work on the analysis of the NCSN catalogue, which not only spans a considerably longer period (44 years between 1968 and 2011), but also appears to be internally consistent.

4.2.2. Analysis of full NCSN catalogue for 1968 – 2011

The analysis of the complete full NCSN catalogue returns stable determinations of $q_M(M_{th})$ which vary from 1.49 to 1.56 (Fig. 10a) and yield b_q in the interval (1.04, 0.79), with larger the q_M (lower b_q) observed at the larger magnitude scales. As can also be seen in Fig. 10b, $q_M(\Delta d)$ determinations are stable in the interval (1.45, 1.53), respectively yielding b_q in the interval (1.22, 0.88).

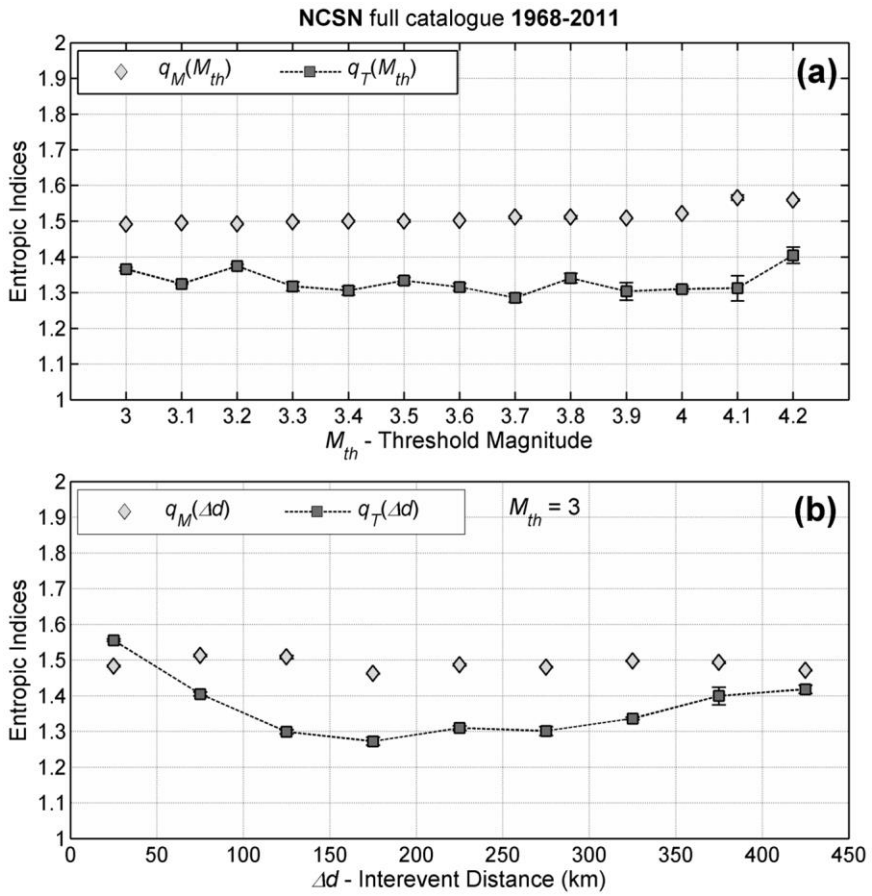

Figure 10. Analysis of the full NCSN catalogue for the 44-year period 1968 – 2011. **(a)** Dependence of entropic indices on threshold magnitude (M_{th}). **(b)** Dependence of entropic indices on interevent distance (Δd); earthquakes are groupped in bins of 50km and symbols are plotted at the midpoint of each bin. In all cases error bars represent 95% confidence intervals.

The temporal entropic indices hold a surprise: $q_T(M_{th})$ is rather consistently determined and found to vary between 1.29 and 1.40 indicating *moderate to high correlation* (Fig. 10a). Moreover, as evident in Fig. 10b, $q_T(\Delta d)$ exhibits a rather *smooth* variation from relatively high correlation (1.55 – 1.40) at short interevent distances (Δd < 100km), which is expected due to the effect of near field interaction, to *moderate correlation* (1.28 – 1.42) at intermediate and long interevent distances (Δd > 100km). The "surprise" is that the temporal entropic indices estimated for the period 1968 – 2011 are generally *higher* than those estimated for the period 1984 – 2011, with particular reference to their variation with respect to interevent distance. Evidently, the differences result from the inclusion (exclusion) of earthquakes observed during the interval 1968 – 1984. This, in turn, indicates that earthquakes prior to mid to late 80's occurred in a (long-range) correlated seismogenetic system and that this correlation was, somehow, relaxed in the years thereafter. Thus, and because correlation implies Criticality, the question reduces to whether it is possible for the seismogenetic system to have switched from the more organized (non-equilibrating) state indicated by Fig. 10 to the less organized state indicated by Fig. 9. A probable "turning point" for such a transition may have been the M7 Loma Prieta earthquake of 17/10/1989. In order to test this hypothesis we have analysed two full NCSN sub-catalogues, the first of which comprises 8289 events and extends from 1968 to 31/12/1988, prior to the Loma Prieta event, and the second of which comprises

4677 events and extends from 1/1/1990, almost 2½ months after the event, to 31/12/2011. The results of this experiment are summarized in Tables 1 and 2, illustrated in Fig. 11 and discussed below.

To begin with, the determination of the magnitude entropic index is *absolutely consistent* between the two periods, so much with respect to threshold magnitude, as with respect to interevent distance: For the period 1968–1988 $q_M(M_{th})$ varies between 1.49 and 1.51 and $q_M(\Delta d)$ between 1.47 and 1.515, while for 1990–2011 $q_M(\Delta d)$ varies between 1.48 and 1.5 and $q_M(\Delta d)$ between 1.46 and 1.51. On the other hand, the temporal entropic indices exhibit markedly different behaviour between the two periods. During the interval 1968-1988 $q_T(M_{th})$ fluctuates between 1.35 and 1.44, indicating moderate overall correlation (Fig. 11a), while $q_T(\Delta d)$ is generally larger than 1.4 and exhibits a persistent upward trend for Δd > 200km, thereby indicating *increasingly higher* correlation at longer interevent distances so that $q_T(\Delta d) > 1.5$ at Δd > 300km (Fig. 11b). Conversely, in the period 1990-2011 $q_T(M_{th})$ decreases gradually from just above 1.2 at $M_{th} < 3.5$ to only 1.12 at $M_{th} = 4$, indicating very weak overall correlation and near randomness at the larger magnitude thresholds (Fig. 11c). Moreover, $q_T(\Delta d)$ is higher than 1.45 at Δd < 100km and indicates high correlation at short interevent distances due to the effect of near-field interactions and aftershock sequences (Fig. 11d); nevertheless, it drops to approx. 1.1 for 100km < Δd < 250km (randomness) and gradually rises to 1.3 at Δd greater than 250km indicating weak to moderate correlation.

The results presented above seem to support the hypothesis that the Loma Prieta event has been a "turning point" in the evolution of North Californian seismicity. Before this earthquake, the regional seismogenetic system appears to have been characterized by a highly organized state involving long range interactions (stress-stress correlations), whereas after the event the level of organization appears to have dropped significantly, with some elements (e.g. larger faults subsystem, intermediate range interactions) having

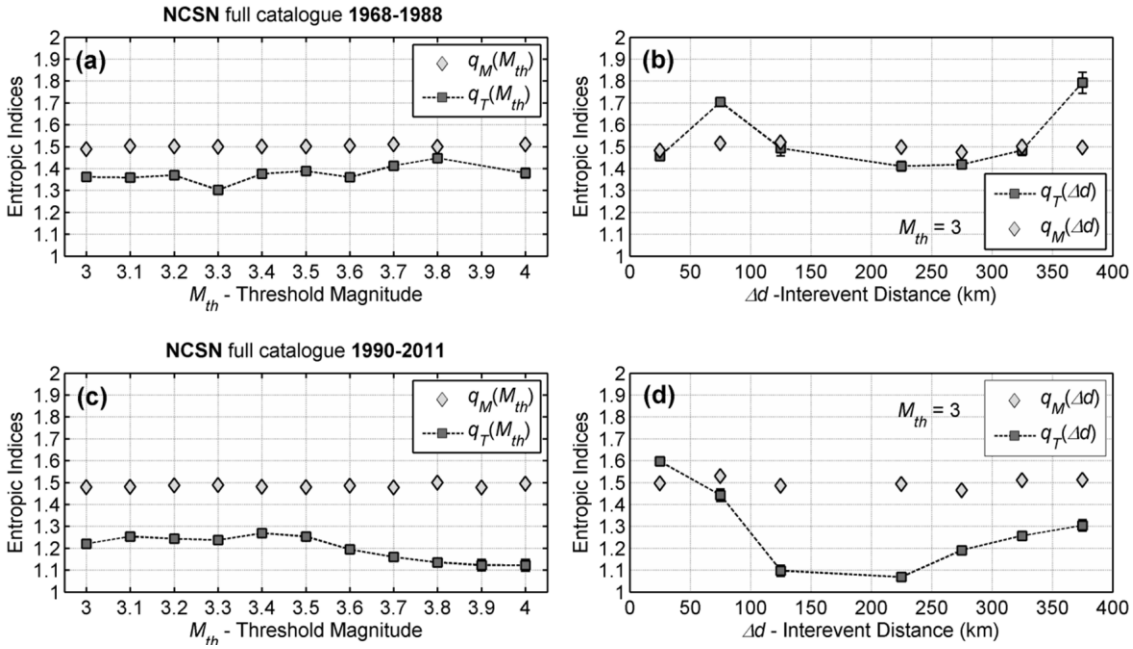

Figure 11. Analysis of the full NCSN catalogue for the periods 1968 – 1988 (top row) and 1990-2011 (bottom row). Panels **(a)** and **(c)** illustrate the dependence of the entropic indices on threshold magnitude (M_{th}). Panels **(b)** and **(d)** illustrate the dependence of the entropic indices on interevent distance (Δd), where earthquakes with groupped in bins of breadth Δd = 50km and symbols are plotted at the midpoint of each bin. Error bars represent 95% confidence intervals.

transited to an almost completely disorganized (random) state. It is also noteworthy that long-range correlation, albeit weakened, appears to have persisted even in the disorganized post Loma Prieta era, as attested to by the increasing trend of $q_T(\Delta d)$ at long interevent distances (ranges): this is an effect characteristic of Criticality.

4.2.3 The north segment of San Andreas Fault and the Sierra Nevada Range for 1968-2011

The next step in our study is to compare the geographically distinct clustering of seismicity along the San Andreas Fault (nSAF) and the Sierra Nevada Range/ Walker Lane belt (SNR). To this effect, we first analyse two subsets of the full NCSN catalogue corresponding to the nSAF and SNR areas, separated as shown in Fig. 4a.

Let us, first, consider the results from the analysis of the nSAF sub-catalogue (Fig. 12). As can be seen in Fig. 12a, the magnitude entropic index $q_M(M_{th})$ exhibits a persistent linear trend from 1.47 at M_{th} = 3 to 1.56 at M_{th} =4.2, with $b_q(M_{th})$ respectively varying from 1.12 to 0.78: If taken at face value, this result would signify gradual change in the scaling of the San Andreas fault system as a function of fault size! The temporal entropic index $q_T(M_{th})$ is invariably larger than 1.2 and fluctuates around a mean value of 1.3 indicating moderate correlation. When earthquakes are grouped by interevent distance, $q_M(\Delta d)$ fluctuates slightly around a mean value of 1.5 (Fig. 12b). Conversely, the temporal entropic index $q_T(\Delta d)$ exhibits variability, being significant (> 1.4) for Δd up to 100 km (near-field effect), rapidly decaying to 1.2 – 1.3 for Δd between 100 and 350 km and, finally, increasing to 1.5 for Δd > 300 km.

Turning to the results from the SNR sub-catalogue (Fig. 12c and 12d), we note that $q_M(M_{th})$ appears to exhibit a (very) low-rate linear trend towards higher values with increasing threshold magnitude,

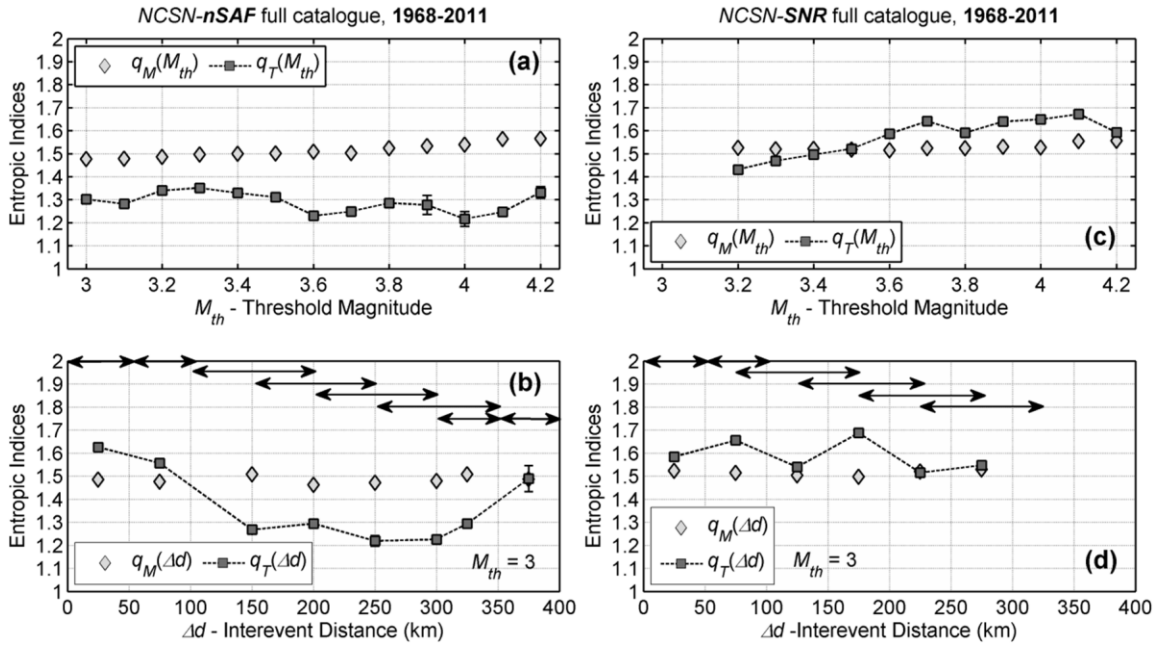

Figure 12: Analysis of the full nSAF catalogue (left column) and SNR catalogue (right column) for the 44-year period 1968-2011. Panels **(a)** and **(b)** illustrate the dependence of the entropic indices on threshold magnitude (M_{th}). Panels **(c)** and **(d)** illustrate the dependence on interevent distance (Δd); the horizontal double arrows indicate the breadth of interevent distance bins and symbols are plotted at the midpoint of each bin. Error bars represent 95% confidence intervals.

conceivably indicating corresponding changes in the scaling of the SNR fault system (Fig. 12c). As it appears that long interevent distances are very rare in the SNR system, the analysis is limited to no more than Δd = 200km (Fig. 12d); as can clearly be seen, $q_M(\Delta d)$ is stable around a mean value of 1.52 ($b_q(\Delta d)$ ~ 0.92). On the other hand, results for the temporal entropic index hold a surprise: as can be seen in Fig. 12c, $q_T(M_{th})$ varies from 1.41 at M_{th} = 3 to 1.67 at M_{th} = 4.2, exhibiting a clear quasi-linear tendency to increase with respect to threshold magnitude, which would be interpreted to signify a corresponding *increase* in the interdependence of earthquake occurrence (correlation) with magnitude and at least up to M = 4.2. Finally, q_T shows moderate to high correlation (1.36-1.66) for all interevent distances up to 200km.

In taking our inquiry one step forward, we examine whether the "turning point" defined by the 1989 Loma Prieta earthquake has affected the nSAF and SNR sub-systems in (dis)similar ways. As per Section 4.2.2, the full NCSN sub-catalogues for the nSAF and SNR areas are analysed separately for the periods 1968-1988 and 1990-2011, that is prior to and after the event. Prior to 1988, the full nSAF sub-catalogue contains 5738 events and the full SNR sub-catalogue 2391 events while after 1990, the corresponding numbers are 2549 and 2284 respectively. It straightforward to see, and certainly significant and worthy of further scrutiny, that the during first 20-year long period the full nSAF sub-catalogue contains almost double the number of events with respect to the second 21-year long period, meaning that there are significant differences in seismicity rates. Conversely, the corresponding numbers in the full SNR sub-catalogue are practically the same (constant seismicity rates?).

Results for the nSAF sub-catalogue are shown in Fig. 13. As evident in Fig 13a, for 1968 – 1988, $q_M(M_{th})$ exhibits a low-rate linear trend from 1.48 at M_{th} = 3 to 1.56 at M_{th} = 4.1; the trend is not apparent in the period 1990 – 2011, where $q_M(M_{th})$ appears to have stabilized just below the value of 1.5, so that at $b_q(M_{th})$

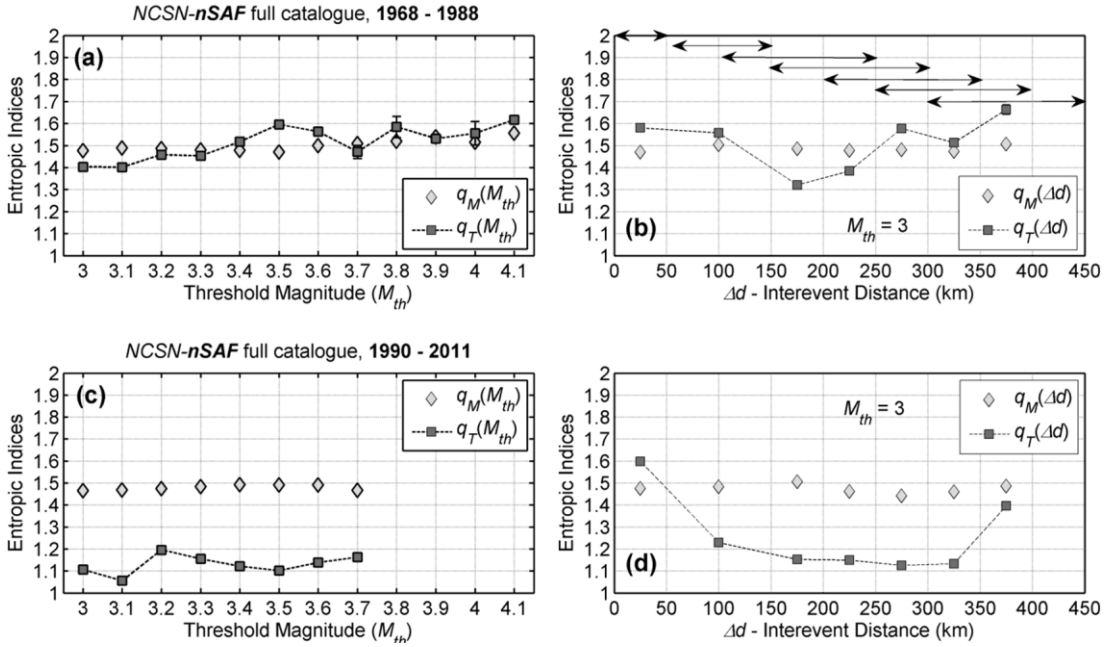

Figure 13. Analysis of the full nSAF catalogue for the periods 1968 – 1988 (top row) and 1990-2011 (bottom row). Panels **(a)** and **(c)** illustrate the dependence of the entropic indices on threshold magnitude (M_{th}). Panels **(b)** and **(d)** illustrate the dependence of the entropic indices on interevent distance (Δd); the horizontal double arrows indicate the breadth of interevent distance bins and symbols are plotted at the midpoint of each bin. Error bars represent 95% confidence intervals.

> 1.1 (Fig. 13c). Note, however, that because the number of earthquakes available for analysis at M_{th} > 3.7 is insufficient, it is not certain whether the "trend" has altogether ceased to exist, or it is simply unobservable. The estimation of magnitude entropic indices with respect to interevent distance is also hampered by the overall insufficient number of events at Δd > 350 km. Observations are necessarily limited to near and intermediate range interaction, where one may observe that $q_M(\Delta d)$ is rather stably determined for both periods, slightly fluctuating about 1.5 (Fig. 13b and 13d). The temporal entropic index exhibits completely different behaviour between the two periods. For 1968 – 1988, $q_T(M_{th})$ displays an upward linear trend, changing from 1.4 at M_{th} = 3 to higher than 1.6 at M_{th} = 4.1 and exhibiting high correlation, particularly at larger threshold magnitudes (Fig. 13a). Significant correlation is also observed in Fig. 13b, where $q_T(\Delta d)$ varies from 1.58 to 1.55 for Δd < 100km and consistently *increases* from 1.39 at Δd between 150-300km, to 1.66 at Δd between 300-450km, indicating high to very high correlation all ranges, with particular reference to long interevent distances (Fig. 13b). For 1990 – 2011 completely different properties are observed: In Fig. 13c $q_T(M_{th})$ is generally lower than 1.15 and $\max[q_T(M_{th})]$ < 1.20: this indicates general absence of significant correlation and a nearly random seismogenetic system. In Fig. 13d, $q_T(\Delta d)$ is 1.59 and exhibits the anticipated high correlation of short interevent distances, but decays rapidly to *under* 1.2 at Δd between 150-350km and rises again to 1.39 at Δd > 350km, thus indicating very weak to no correlation at intermediate ranges but moderate correlation at long ranges.

Results for the full SNR sub-catalogue are presented in Fig. 14 and hold their own surprises. As can be seen in Fig. 14a, for the period 1968 – 1988, $q_M(M_{th})$ is very consistently determined at approx. 1.55 for all threshold magnitudes, yielding a correspondingly consistent $b_q(M_{th})$ of approx. 0.82. For the 1990 – 2011, and save for the last two threshold magnitudes, $q_M(M_{th})$ is also consistently determined but with

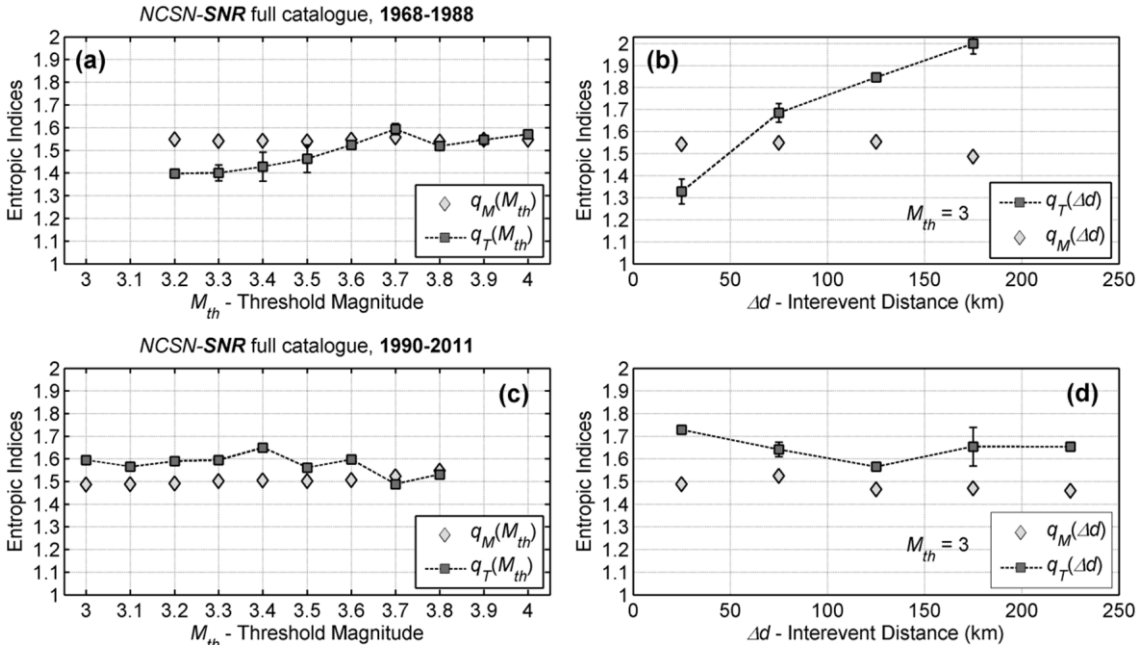

Figure 14. Analysis of the full SNR catalogue for the periods 1968 – 1988 (top row) and 1990-2011 (bottom row). Panels **(a)** and **(c)** illustrate the dependence of the entropic indices on threshold magnitude (M_{th}). Panels **(b)** and **(d)** illustrate the dependence of the entropic indices on interevent distance (Δd), where earthquakes with groupped in bins of breadth Δd = 50km and symbols are plotted at the midpoint of each bin. Error bars represent 95% confidence intervals.

values just below, or approximately equal to 1.5 so that $b_q \approx 1$ (Fig. 14c). Although it is not easy to make safe inferences, this might signify a change in the scaling of the active tectonic grain. Analogous observations can be made by comparing $q_M(\Delta d)$ prior to 1988 (Fig. 14b) and after 1990 (Fig. 14d). Turning to the analysis of the temporal entropic index, we note that for the period 1968 – 1988, $q_T(M_{th})$ varies from 1.4 at M_{th} = 3 to 1.59 at M_{th} = 4, indicating significant to high correlation (Fig. 14a). Moreover, it exhibits an upward linear trend analogous to that observed in Fig. 13a for the corresponding analysis of the nSAF sub-catalogue. For the period 1990 – 2011, $q_T(M_{th})$ is consistently *higher* than 1.5 but is *no longer* increasing with threshold magnitude (Fig. 14c). Analogous observations can be made with respect to interevent distances, although this analysis is somewhat hampered by insufficient numbers of events for Δd longer than 250 km. For the first period $q_T(\Delta d)$ exhibits persistent and strong increase from 1.33 at Δd < 50km to 1.84 at Δd > 150km, indicating *increasingly* strong correlation at intermediate and long ranges (Fig.14b). For the second period (1990 – 2011) $q_T(\Delta d)$ varies from 1.73 at Δd < 50km to 1.57 at Δd > 200km indicating *persistently high* correlation at *all* ranges which, however, is *no longer* increasing with interevent distance (Fig. 14d). Overall, it appears that although something has changed, the SNR fault system remained highly correlated both prior to and after the Loma Prieta event and, more significantly, it is statistically *different* from the nSAF system!

4.3. Declustered catalogues

A primary objective of our study is to investigate whether background seismicity is generated by non-Poissonian dynamic processes. Accordingly, we shall now proceed to examine reduced versions of the NCSN, nSAF and SNR catalogues, in which aftershock sequences have been identified and removed by the stochastic declustering method of Zhuang et al (2002) at the $\phi_j(\geq 0.7)$, $\phi_j(\geq 0.8)$ and $\phi_j(\geq 0.9)$ probability levels (i.e. probability greater or equal to 70%, 80% and 90% for an event to belong to the background). It is important to note that the analysis of entropic indices with respect to interevent distance will be limited to the NCSN catalogue and only to the case $\phi_j(\geq 0.7)$. In all other realizations of the declustered catalogues, the analysis will focus on the study of $q_M(M_{th})$ and $q_T(M_{th})$ because the overall small populations of events at interevent distances longer than 50km may not warrant the statistical significance of $q_M(\Delta d)$ and $q_T(\Delta d)$.

Fig. 15 illustrates the results obtained from the NCSN catalogue, declustered at the $\phi_j(\geq 0.7)$ or 70% probability level. Specifically, Fig. 15a shows the variation of the entropic indices with threshold magnitude and Fig. 15b the analogous variation with interevent distance. We note that for Δd > 50km, the entropic indices had to be determined in variable-width Δd-bins so as to ensure their statistical significance; the span of the Δd-bins is indicated with horizontal double-headed arrows and, as before, symbols are plotted at the midpoint of each bin. It is immediately apparent that $q_M(M_{th})$ changes smoothly from 1.51 to 1.55 and exhibits the familiar tendency to increase with threshold magnitude (Fig 15a). However, $q_M(\Delta d)$ exhibits a peculiar albeit smooth oscillation with increasing interevent distance, which we will not endeavour to explain in physical terms (e.g. fault scaling) for lack of sufficient evidence. Next, we note that with only one exception at M_{th} = 3.7, $q_T((M_{th})$ is consistently determined at values greater than 1.4, so that $\bar{q}_T(M_{th}) = 1.45 \pm 0.06$; this is definitely higher than the corresponding value obtained for the full NCSN catalogue (1.33 ± 0.033). Given that for the most part aftershocks have been eliminated at the 70% probability level, this increase may be taken to indicate an overall correlated seismogenetic background. Analogous observations can be made on the behaviour of $q_T(\Delta d)$. Thus, for $\Delta d \leq$ 50km, q_T is 1.86, which is higher than the corresponding determination of the full NCSN catalogue by approx. 0.3. It is therefore conceivable that this increase signifies the existence of strong short-range (near

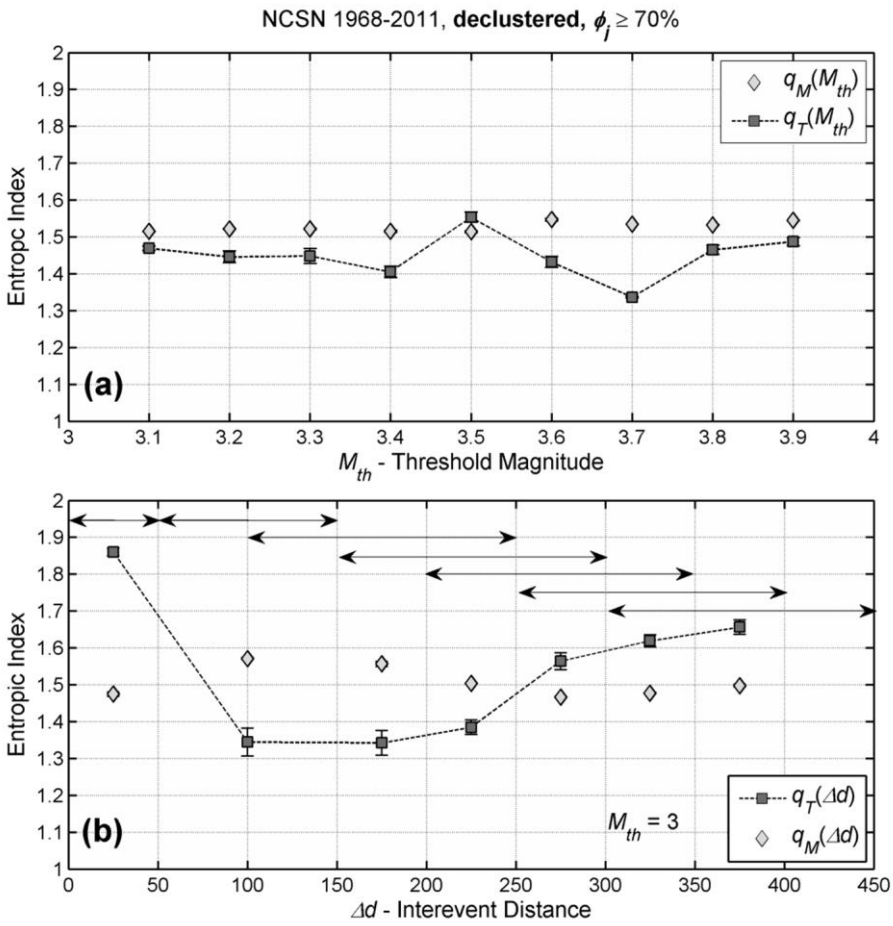

Figure 15. Analysis of declustered ($\phi \geq 70\%$) NCSN catalogue for the 44-year period 1968 – 2011. **(a)** Dependence of entropic indices on threshold magnitude (M_{th}). **(b)** Dependence of entropic indices on interevent distance (Δd); the horizontal double arrows indicate the breadth of interevent distance bins and symbols are plotted at the midpoint of each bin. Error bars represent 95% confidence intervals thoughout.

field) correlation in background seismicity. Likewise, for $\Delta d \geq 200$km q_T averages to 1.61 which is higher by 0.26 in comparison to the corresponding determination for the full NCSN catalogue. It is again conceivable that this increase signifies the existence of rather strong long-range (far field) correlation in the background.

Let us, now, examine the nSAF and SNR catalogues declustered at the $\phi_j(\geq 0.7)$ level, for which results are shown in Fig 16a (nSAF) and Fig. 16b (SNR). It is apparent that $q_M(M_{th})$ determinations are very stable for both catalogues and exhibit minimal variation, so that for the declustered nSAF catalogue $\bar{q}_M(M_{th}) = 1.51 \pm 0.014$ ($b_q = 0.96$) and for the SNR catalogue $\bar{q}_M(M_{th}) = 1.55 \pm 0.007$ ($b_q = 0.81$): the two mean entropic indices stand apart of each other by more than two standard errors, which may indicate different scaling of earthquake (fault) sizes in the two areas. More interesting observations can be made in regard to the temporal entropic index. For the nSAF catalogue q_T varies between 1.41 and 1.60 with an average of 1.48, while for SNR q_T varies between 1.73 and 1.83 with an average of 1.78. Such values indicate that background processes at the respective seismogenetic systems are highly and very highly correlated and, more significantly, at levels higher than those estimated from the combined (NCSN) catalogue.

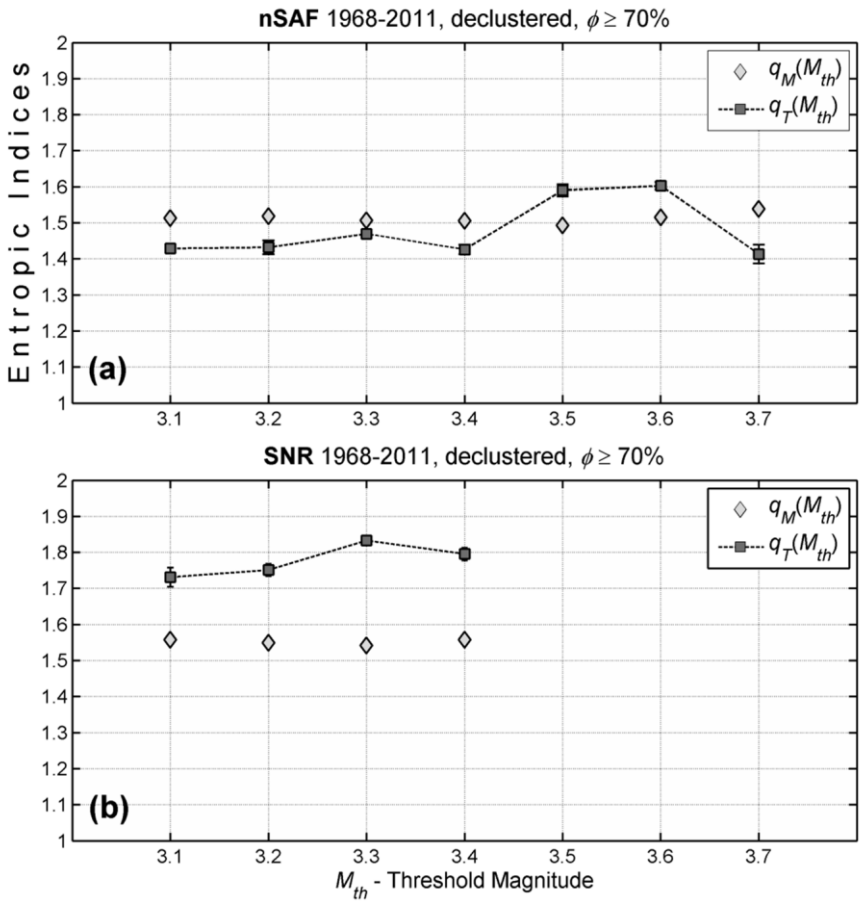

Figure 16. Dependence of entropic indices on threshold magnitude (M_{th}) over the 44-year period 1968 – 2011 for **(a)** the declustered ($\phi \geq 70\%$) nSAF catalogue and, **(b)** the declustered SNR catalogue. Error bars represent 95% confidence intervals.

The hitherto analysis of the declustered catalogues yields temporal entropic indices which indicate correlation invariably higher than that inferred from the full catalogues, therefore strongly non-Poissonian background seismogenetic processes. Still, as already noted in Section 3.1, at the 70% probability level the declustered catalogues contain a certainly non-trivial number of leftover aftershocks. Accordingly, it is essential to show that the results obtained at this level hold, or even improve at higher probability thresholds.

The analysis of the NCSN and nSAF catalogues declustered at probability levels $\phi_j \geq 80\%$ and $\phi_j \geq 90\%$ to be background, as well as of the SNR catalogue declustered at probability $\phi_j \geq 80\%$ to be background, is summarized in Table 1. The SNR catalogue declustered at $\phi_j \geq 90\%$ contains only 214 events and may not be reliably evaluated. In addition, the variations of $\overline{q}_M(M_{th})$ and $\overline{q}_T(M_{th})$ for the full and declustered NCSN, nSAF and SNR catalogues at different probabilities are shown in Fig. 17a and 17b respectively, with values corresponding to the full catalogues nominally plotted at the abscissa $\phi_j = 0$.

Inspection of Table 1 and Fig. 17a shows that $\overline{q}_M(M_{th})$ exhibit very little variation with increasing probability. However it is also interesting to note that results are distinctly different for the nSAF and SNR areas, possibly reflecting differences in the scaling of the respective active fault systems, with their combination (NCSN) comfortably plotting in between! Conversely, inspection of Table 1 and Fig. 17b

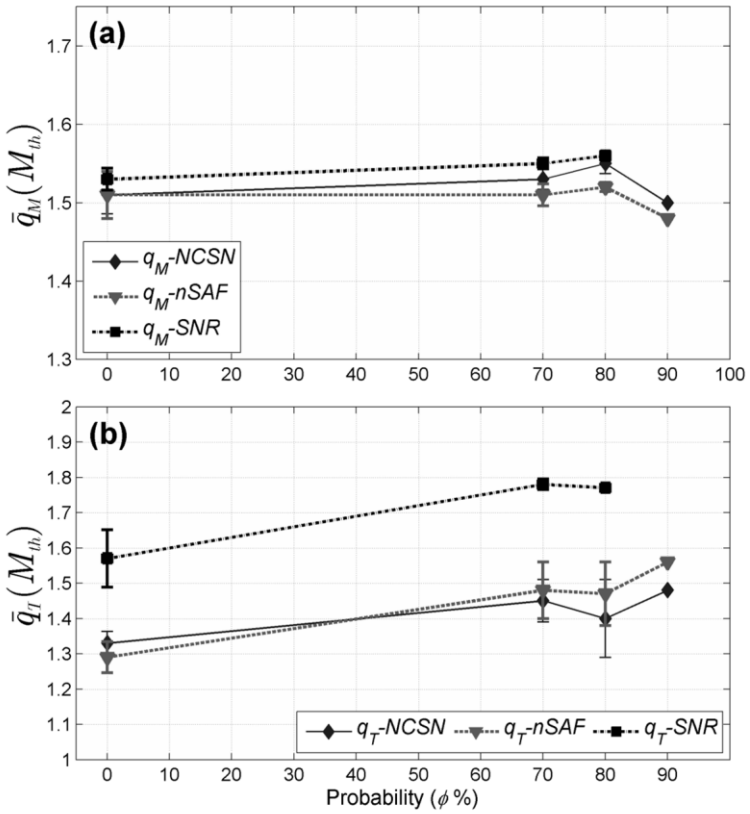

Figure 17. Variation of **(a)** the mean magnitude entropic index and **(b)** the mean temporal entropic index for the full and declustered (at different probability levels) NCSN, nSAF and SNR catalogues. Values corresponding to the full catalogues are nominally plotted at the abscissa $\phi_t = 0$ (zero probability level).

shows that $q_T(M_{th})$ and $\bar{q}_T(M_{th})$ in particular, exhibit *clear* increase with increasing probability to be background and that the nSAF and SNR areas are *significantly* different. Thus, $\bar{q}_T$-nSAF changes from 1.29 for full catalogue to 1.56 for the version declustered at the 90% probability level, while $\bar{q}_T$-SNR changes from 1.57 for the full catalogue to 1.77 for the version declustered at the 80% probability level. Their combination, reflected in the variation of $\bar{q}_T$-NCSN, changes from 1.33 for the full catalogue to 1.48 for the realization declustered at the 90%.level and exhibits more "random" a nature, presumably in consequence of mixing two earthquake populations with distinctly different temporal dynamics.

Our analysis has shown that on removing aftershock sequences, increased correlation is observed! All catalogues considered herein yield q_T values that would render the seismogenetic system(s) of North California definitely non-Poissonian. Moreover, the dynamics of the nSAF and SNR sub-systems are distinctly different: The SNR system exhibits very high correlation (very long memory and very long-range interaction) to the point that any earthquake anywhere in the system would appear to influence the occurrence of future events. To a lesser degree, the same is true for the north segment of the San Andreas Fault system, with the difference that SNR appears to evolve in a perennial state of high correlation, while nSAF has demonstrated a dynamic transition from higher to lower non-equilibrating states in reference to the Loma Prietta event; this outcome also indicates that different driving (seismogenetic) mechanisms operate at those two areas.

5. Discussion and Conclusions

It is generally accepted that seismicity results comprises the superposition of a background process expressing the continuum of tectonic deformation and a foreground process comprising large populations of triggered events and aftershock sequences (short-term activity associated with individual background events). There are two general points of view as to the nature of background (core) seismogenesis: either it is a self-excited conditional Poisson (point) process, or it is Complex with Self-Organized Criticality being the most probable driving mechanism. In the former case, core earthquakes would be spontaneously generated in the seismogenetic continuum and would be independent of each other. Accordingly, there should be no correlation (dependence) between background events; the statistical mechanics of background seismogenesis should obey the Boltzmann-Gibbs formalism and its observed statistical properties should bear evidence of extensivity. In the latter case, long-range interactions in non-equilibrium states are expected, so that background events should be correlated (interdependent) and the statistical mechanics of background seismogenesis should be non-extensive, significantly deviating from the Boltzmann-Gibbs formalism. Both points of view agree that foreground earthquakes, which are genetically related to their parent event, comprise correlated sets. It follows that if were possible to identify and remove aftershocks, it would also be possible to investigate the nature of the seismogenetic system by examining background earthquakes for the existence of correlation.

In the present study we examine the nature of the seismogenetic system(s) of North California, USA, by searching for evidence of complexity and non-extensivity in the seismicity record. Specifically, we search for signs of long-range interaction and correlation in bivariate cumulative distributions of earthquake magnitudes and interevent times, based on the formalism of Non-Extensive Statistical Physics, (e.g. Tsallis, 1988, 2009), that generalizes Boltzmann-Gibbs thermodynamics to non-equilibrating complex systems. The search is performed for the period 1968 – 2011 during which earthquake catalogues are homogeneous and complete for $M_L \geq 3$, with aftershocks sequences either included (full catalogues), or eliminated (declustered catalogues) using the stochastic declustering method of Zhuang et al (2002, 2004).

The existence of "correlation" is assessed by estimating and evaluating the magnitude (q_{M}) and temporal (q_{T}) entropic indices, which indicate the level on non-equilibrium or, equivalently, the extent of interaction and inter-dependence in a complex system (see Sections 2 and 4). The magnitude entropic index shows that the size distribution of active faults is absolutely consistent with the empirical G-R law and yields proxy *b*-values consistent with empirical *b*-value determinations based on conventional estimation procedures. Specifically, q_M generally varies in the rather limited range of 1.45 to 1.56 for both full and declustered catalogues, so that the application of Eq. 18 yields proxy *b*-values in a range of 1.22-0.78. In comparison, conventional estimation procedures yield $b \in (1.18 - 0.75)$. This is important because in the context of Boltzmann-Gibbs thermodynamics (random processes) the G-R law is empirical and *cannot* be derived from first principles. Conversely, it *can* be derived from first principles in the more general context of NESP thermodynamics. Accordingly, not only are the results obtained on the basis NESP compatible with the well-understood concept of scale-free organization in the size and geometry of the active fault system(s), but their equivalence to conventionally estimated *b* values also indicates that said system(s) can be classified as sub-extensive complex with a high degree of self-organization.

The temporal entropic index (q_T) indicates the extent to which earthquake events may stimulate the occurrence of their successors over a broad range of distances. By analysing numerous Poissonian synthetic background catalogues constructed on the basis of the ETAS model, we have demonstrated that truly random seismicity processes should yield q_T generally less than 1.1 and that $q_T + 3\sigma < 1.2$ (see Fig. 8a). This defines the threshold above which it is safe to assume non-Poisson statistical physics. For the

period studied herein and excluding the area of Mendocino Triple Junction, the seismicity of North California generally yields $q_T > 1.2$ and appears to be generated by two sub-extensive subsystems with rather different characteristics: the central and northern segments of the San Andreas Fault, (nSAF) and the Sierra Nevada Range – Walker Lane (SNR).

The nSAF system exhibits moderate to high level of correlation that varies with time and specifically with respect to the landmark Loma Prieta event. More precisely, the analysis of the full nSAF catalogue for the period leading to the Loma Prieta event and for different threshold (cut-off) magnitudes M_{th} yields $q_T(M_{th})$ in the range 1.4–1.62 and $\bar{q}_T(M_{th}) = 1.51 \pm 0.074$, while for the period after the Loma Prieta event yields $q_T(M_{th}) \leq 1.2$ with $\bar{q}_T(M_{th}) = 1.13 \pm 0.043$. These differences are likely to be associated with changes in seismicity rates before and after Loma Prieta: In the period 1968 – 1988, 5736 were observed along nSAF. In the period 1990-2011, the number drops to only 2391 events, less than half the previous. At the same time, the seismicity rate after 1990 is apparently decreasing for both the full and declustered catalogues (Fig. 7).

Conversely, the SNR system exhibits high to very high levels of correlation: Analysis of the complete SNR catalogue (1968 – 2011) for different threshold magnitudes yields $q_T(M_{th}) \in (1.43 – 1.67)$ and $\bar{q}_T(M_{th}) = 1.51 \pm 0.074$, while for the period leading to the Loma Prieta event $q_T(M_{th}) \in (1.4 – 1.59)$ with $\bar{q}_T(M_{th}) = 1.49 \pm 0.074$ and for the period after the event $q_T(M_{th}) \in (1.48 – 1.65)$ with $\bar{q}_T(M_{th}) = 1.57 \pm 0.046$. Likewise, the seismicity rates appear to remain approximately constant with 2549 events in the interval 1968-1988 and 2284 events in the interval 1990-2011. This indicates that the correlation level is persistently high so that the SNR fault system evolves in a state of perennial strong non-equilibrium that is marginally influenced by processes taking place along the nSAF (if at all). It also points to fundamentally different mechanisms underlying the seismicity of nSAF and SNR.

A most interesting observation is that as can clearly be seen in Table 1 and Fig. 10-17, on removing aftershock sequences increased $q_T(M_{th})$ values (correlation) are observed throughout, an effect also observed by Efstathiou et al. (2015). Although this effect requires additional and rigorous investigation, a plausible explanation is that because foreground processes are localized in time and space, their removal unveils the existence of long-range interactions in the background process, which their presence otherwise obscures. What is also important to point out is that ETAS-based parametric stochastic declustering *fails* to reduce the catalogue to a sequence of independent events. We consider useful to elaborate on this point because van Stiphout et al (2012) have presented comparisons of declustering algorithms in which they applied the χ^2 goodness of fit test to determine whether the background seismicity recovered by any given algorithm comprised a random sequence of events with respect to their time of occurrence (null hypothesis). They found that at the 5% significance level, the methods of Zhuang et al. (2002) and Marsan and Lengliné (2008) yielded sequences that followed Poisson distributions in time, although the corresponding estimated sets of background earthquakes differed considerably in absolute numbers. On these grounds, they have also hinted that Poisson processes are in control of background seismicity. We contend that this (and analogous) tests can be misleading because absolute occurrence times do not relate earthquakes with their predecessor and successor events so that the distribution of occurrence times *cannot* yield a measure of interaction, or of the distance over which interaction may take place. On the other hand, the distribution of interevent times does, as explained in the foregoing. Thus, when viewed in the context of NESP, our results indicate that background seismicity throughout North California expresses an ensemble of persistently sub-extensive systems!

Significant observations are also made upon examination of earthquake sub-catalogues separated (grouped) according to interevent distance (Δd), so as to explicitly test for operational long-range correlation. The analysis of the full NCSN catalogue shows that high correlation ($q_T(\Delta d) > 1.5$) is generally observed at short interevent distances ($\Delta d < 100$km), an effect that can easily be explained by the overwhelming effect of (clustered and correlated) aftershock sequences. Nevertheless, intermediate correlation $q_T(\Delta d) \in (1.25 - 1.35)$ is also observed at intermediate interevent distances (of the order of 100 – 250km) and, more significantly, intermediate-high correlation ($q_T(\Delta d) > 1.35$) is observed at *long* interevent distances ($\Delta d > 250$km). Moreover, declustering appears to *increase* correlation at *short* and *long* interevent distances. Differences in the dynamic expression of seismicity between the nSAF and SNR subsystems are also observed and are analogous to those discussed above. Specifically, in the nSAF, the level of correlation with respect to interevent distance changes significantly in reference to the Loma Prieta event: Prior to this earthquake, the correlation is above moderate at all interevent distances ($q_T(\Delta d) > 1.3$) and rather high ($q_T(\Delta d) > 1.5$) at short and long Δd; after the earthquake correlation is high only the shortest interevent distance group ($\Delta d < 50$km) and drops to under 1.2 for intermediate interevent distances ($50\text{km} < \Delta d < 300\text{km}$) only to rise to moderate levels ($q_T(\Delta d) = 1.4$) for the longest interevent distance group ($\Delta d > 300$km). Conversely, in the SNR system correlation is generally high for all interevent distance groups, both before and after the Loma Prieta event; it is nevertheless worth noting that during 1968-1988 correlation appears to increase as Δd increases, to remarkably high levels!

The results presented above have been obtained through a physics-based approach (NESP) and *not* through any type of model-based (or model-driven) consideration, as usually is the case in earthquake statistical studies. They provide strong evidence that the seismogenetic system(s) of North California are definitely complex sub-extensive and certainly non-Poissonian of nature. Background seismicity exhibits long-range interaction as evident in the overall increase of correlation in the declustered catalogues and, primarily, in the high correlation observed for earthquakes separated by long interevent distances, with particular reference to the nSAF system. The increase of correlation after declustering can be neatly explained by the exposition of long(er) range interactions after curtailing the effect of short-range interactions associated with aftershock sequences. Moreover, even for the full (clustered) earthquake catalogues, the high correlation observed at long interevent distances can hardly be explained in terms of aftershock sequences, since interevent distances of the order of 200km are several times longer than aftershock zones associated with M_w 6 – 6.7 earthquakes and significantly longer than zones associated with M_w 7-7.2 earthquakes (e.g. Kagan, 2002). Therefore, it is more reasonable to argue in favour of operational long-range interaction.

Inasmuch as long-range interaction is characteristic of self-organization and criticality, it is also important to emphasize that two SO subsystems with rather different properties appear to exist in North California: the Sierra Nevada Range – Walker Lane subsystem is stationary in time and has attributes of Self-Organized Criticality as described in Bak and Tang (1989), Sornette and Sornette (1989), Olami et al. (1992), Bak et al. (2002), Bakar and Tirnakli (2009) and many others. Conversely, the north segment of the San Andreas Fault (nSAF) exhibits changes in the level of self-organization with respect to the large Loma Prieta event and thus has attributes of Critical Point behaviour (Self-Organizing Criticality), albeit without evident acceleration of seismic release rates as predicted by some CP models (e.g. Sornette and Sammis, 1995; Rundle et al., 2000; Sammis and Sornette, 2001).

At this point we should note that although SO Criticality appears to be a very likely explanation of the complexity mechanism, the question is still far from having been definitively dealt with. As comprehensively discussed by Sornette and Werner (2009), complexity may not only emerge from

inherent non-linear dynamics of the active fault system as required by Criticality– their model-driven analysis suggests that quenched heterogeneity in the stress field and production rates may also be of great importance. It is also noteworthy that using the non-critical Coherent Noise Model, Celikoglu et al. (2010) showed that it is possible to obtain *q*-exponential distributions of interevent times when extended external stresses act simultaneously and coherently on all the elements of a fault system. Although this does not explain the differences of the nSAF and SNR systems, it is clear that additional work is required before a complexity mechanism of the background seismicity can be proposed with confidence. At any rate, we believe that we have enough evidence to put forward some ideas as to the nature and possible origin of SO Criticality in North California.

To begin with, it is well-appreciated that active fault networks are *non-conservative* systems, inasmuch as friction is a non-conservative force. This property and the herein documented existence of long-range interaction and possibly critical state, in association with studies based on small-world Olami-Feder-Christensen models (Caruso et al., 2005; Caruso et al., 2007) point to a *small-world topology* for the fault networks of North California. In such networks each fault is a node that belongs to a local cluster where it occupies some hierarchical level according to its size and interacts with local or distal faults (nodes) according to the respective connectivity and range of its hierarchical level. Upon excitation by some (slow or fast) stress perturbation, a node responds by storing (accumulating) energy in the form of strain and subsequently transmitting it to *connected* nodes or/and releasing it at various rates; in other words, it operates as a delayed feedback loop.

Now, consider that the hierarchy and spatial distribution of the active fault network is not only fractal as attested to by the Gutenberg–Richter Law, but also sub-extensive as demonstrated herein, by laboratory experiments (e.g. Vallianatos et al., 2012b) and by relevant research (Vallianatos and Sammonds, 2011; Michas et al., 2015; references in Section 2.2). The distribution of stress across the network is heterogeneous and so are stress transfer and release rates (delayed feedback). Finally and perhaps more importantly, the network is subject to open boundary conditions at the Earth-Atmosphere interface so that top-tier faults, which in transformational tectonic settings almost certainly break at the surface, comprise boundary elements of the network. It is documented that in Olami-Feder-Christensen networks, open boundary conditions compel the boundary elements to interact at a different (delayed) frequency with respect to the bulk of elements buried deeper in the crust and that this inhomogeneity induces partial synchronization of the boundary elements, building up long range correlation and facilitating the development of a critical state (e.g. Lise and Paszucki; Caruso et al., 2005; Hergarten and Krenn, 2011). This effect should also be accentuated by heterogeneity and delayed feedback across the entire network, which also appear to be important for the development of criticality in small-world networks (Yang, 2001; Caruso et al., 2007).

In conclusion, it is plausible that the small-world character and sub-extensive critical state of the fault network in North California is induced by the high connectivity of synchronised top-tier faults, as for instance are the contiguous segments of the nSAF. These operate as "hubs" that facilitate longitudinal interactions (transfer of stress) between distal clusters but inhibit transverse interactions between distal *networks*, as for instance between nSAF and SNR. The intensity of the longitudinal interactions may vary in response to time-dependent changes in stress/strain heterogeneity and connectivity (stress level) of the hubs, as for instance, may have happened before and after the Loma Prietta event. The view posits that open boundary conditions are key to the development of complexity and criticality. By inference, it also implies that deep-seated fault networks, as for instance those in Wadati-Benioff zones, should be kept away from criticality as they are subject to closed boundary conditions (no fault synchronization). If our interpretation holds water, interevent time distributions of sub-crustal earthquakes should be thin-tailed

power-law, or even purely exponential (random). This, however, remains to be demonstrated with future research.

6. Acknowledgments

We acknowledge many useful exchanges of ideas with Dr Margaret Segou of the British Geological Survey, Edinburgh. This work was partly supported by the THALES Program of the Ministry of Education of Greece and the European Union in the framework of the project "Integrated understanding of Seismicity, using innovative methodologies of Fracture Mechanics along with Earthquake and Non-Extensive Statistical Physics – Application to the geodynamic system of the Hellenic Arc - SEISMO FEAR HELLARC".

7. References

Abe, S., and N. Suzuki 2005. Scale-free statistics of time interval between successive earthquakes. *Physica A*, 350, 588-596.

Abe, S., Suzuki, N., 2003. Law for the distance between successive earthquakes, *J. Geophys. Res*., 108 (B2), 2113.

Antonopoulos C.G., Michas G., Vallianatos F. and Bountis T., 2014. Evidence of q-exponential statistics in Greek seismicity. *Physica A: Statistical Mechanics and its Applications*, 409, 71-77; doi: 10.1016/j.physa.2014.04.042

Bak, P. and C. Tang, 1989. Earthquakes as a self-organized critical phenomenon. *J. Geophys. Res.*, 94, 15635-15637.

Bak, P., Christensen, K., Danon, L. and Scanlon, T., 2002. Unified scaling law for earthquakes, *Phys. Rev. Lett.*, 88, 178501; doi:10.1103/PhysRevLett.88.178501.

Bakar, B. and Tirnakli, U., 2009. Analysis of self-organized criticality in Ehrenfest's dog-flea model, *Phys. Rev. E*, 79, 040103; doi:10.1103/PhysRevE.79.040103.

Batak R. C and Kantz H., 2014. Observing spatio-temporal clustering and separation using interevent distributions of regional earthquakes, *Nonlin. Processes Geophys*., 21, 735–744; doi:10.5194/npg-21-735-2014.

Beck, C. and Schloegl, F., 1993. *Thermodynamics of Chaotic Systems: An Introduction,* Cambridge University Press, Cambridge University Press, pp. 88-93.

Becker T.W., Hardebeck J.L. and Anderson G., 2005. Constraints on fault slip rates of the southern California plate boundary from GPS velocity and stress inversions, *Geophys. J. Int.*, 160 (2), 634–650.

Carbone, V., Sorriso-Valvo, L., Harabaglia, P. and Guerra, I., 2005. Unified scaling law for waiting times between seismic events, *Europhys. Lett.*, 71 (6), 1036; doi: 10.1209/epl/i2005-10185-0.

Caruso, F., Latora, V., Rapisarda, A. and Tadić, B., 2005. The Olami-Feder-Christensen model on a small-world topology, arXiv:cond-mat/0507643v1 [cond-mat.stat-mech] (last accessed April 2017).

Caruso, F., Pluchino, A., Latora, V., Vinciguerra, S. and Rapisarda, A., 2007: Analysis of self-organized criticality in the Olami-Feder-Christensen model and in real earthquakes, *Phys. Rev. E*, 75, 055101; doi: 10.1103/PhysRevE.75.055101.

Celikoglu, A., Tirnakli, U., and Duarte Queirós, S., 2010. Analysis of return distributions in the coherent noise model, *Phys. Rev. E*, 82, 021124; doi:10.1103/PhysRevE.82.021124.

Corral, A., 2004. Long-term clustering, scaling, and universality in the temporal occurrence of earthquakes, *Phys. Rev. Lett.*, 92, 108501.

Darooneh, A.H. and Dadashinia, C., 2008. Analysis of the spatial and temporal distributions between successive earthquakes: Nonextensive statistical mechanics viewpoint, *Physica A*, 387, 3647-354.

Darooneh, A.H. and Mehri, A., 2010. A nonextensive modification of the Gutenberg_Richter law: q-stretched exponential form, *Physica A*, 389, 509-514, doi:10.1016/j.physa.2009.10.006.

Davidsen, J. and Goltz, C., 2004. Are seismic waiting time distributions universal? *Geophys. Res. Lett.*, 31, L21612; doi 10.1029/2004GL020892.

Dixon, T.H., Miller, M., Farina, F., Wang, H., and Johnson, D., 2000. Present-day motion of the Sierra Nevada block and some tectonic implications for the Basin and Range province, North American Cordillera, *Tectonics*, 19, 1–24; doi: 10.1029/1998TC001088.

Dengler, L., Moley, K., McPherson, R., Pasyanos, M., Dewey, J.W. and Murray, M.H., 1995. The September 1, 1994 Mendocino fault earthquake, *California Geology* 48, 43 – 53.

Eaton J.P., 1992. Determination of amplitude and duration magnitudes and site residuals from short-period seismographs in Northern California, *Bull. Seism. Soc. Am.*, 82 (2), 533-579.

Efstathiou A., Tzanis A. and Vallianatos, F, 2015. Evidence of Non-Extensivity in the evolution of seismicity along the San Andreas Fault, California, USA: An approach based on Tsallis Statistical Physics, *Phys. Chem. Earth, Parts A/B/C*, 85–86, 56–68; doi:10.1016/j.pce.2015.02.013.

Efstathiou A., Tzanis, A. and Vallianatos F., 2016. On the nature and dynamics of the seismogenetic system of South California, USA: an analysis based on Non-Extensive Statistical Physics, *Bull. Geol. Soc. Greece*, **L** (3), 1329-1340; available online http://www.geosociety.gr/images/news_files/EGE_L/EGE2016_Proceedings_Volume_L_3.pdf (last accessed April 2017).

Eneva M. and Pavlis L. G, 1991. Spatial Distribution of Aftershocks and Background Seismicity in Central California, *Pure and Applied Geophysics*, 137 (1), 35-61.

Felzer, K. R. and Brodsky, E. E. 2006 Evidence for dynamic aftershock triggering from earthquake densities, *Nature*, 441, 735-738.

Felzer, K. R., 2007. Stochastic ETAS Aftershock Simulator Program (AFTsimulator), available at http://pasadena.wr.usgs.gov/office/kfelzer/AftSimulator.html; last access 20 October 2014.

Felzer, K. R., Becker, T. W., Abercrombie, R. E. , Ekstrom, G. and Rice J. R., 2002. Triggering of the 1999 Mw 7.1 Hector Mine earthquake by aftershocks of the 1992 Mw 7.3 Landers earthquake, *J. Geophys. Res.*, 107, 2190; doi:10.1029/2001JB000911.

Fialko Y., 2006. Interseismic strain accumulation and the earthquake potential on the South San Andreas fault system, *Nature*, 441; doi:10.1038/nature04797, 968-971.

Gardner, J. K., and Knopoff, L., 1974. Is the sequence of earthquakes in Southern California, with aftershocks removed, Poissonian? *Bull. Seism. Soc. Am.*, 64 (5), 1363-1367.

Gell-Mann, M. and Tsallis, C. (eds.), 2004. *Nonextensive Entropy – Interdisciplinary Applications*. Oxford University Press, New York.

Goter, S.K., Oppenheimer, D.H., Mori, J.J., Savage, M.K., and Masse, R.P., 1994. Earthquakes in California and Nevada, U.S. Geological Survey Open-File Report 94-647, scale 1:1,000,000, 1 sheet.

Hammond W. C. Blewitt G., Li Z., Plag H.-P. and Kreemer C., 2012. Contemporary uplift of the Sierra Nevada, western United States, from GPS and InSAR measurements, *Geology*, 40 (7), 667-770; doi:10.1130/G32968.1.

Hainzl, S., Scherbaum, F. and Beauval, C., 2006. Estimating background activity based on interevent-time distribution, *Bull. Seismol. Soc Am.*, 96 (1), 313–320; doi: 10.1785/0120050053.

Hardebeck, J. L., and. Hauksson E., 2001. Crustal stress field in southern California and its implications for fault mechanics, *J. Geophys. Res.*, 106, 21,859–21,882.

Hawkes, A.G. 1972. Spectra of some mutually exciting point processes with associated variables, in P.A.W. Lewis (ed), *Stochastic Point Processes*, Wiley, 261-271.

Hawkes, A.G. and Adamopoulos, L., 1973. Cluster models for earthquakes - regional comparisons, *Bull Internat. Stat. Inst.*, 45, 454-461.

Hawkes, A.G. and Oakes, D., 1974. A cluster representation of a self-exciting process, *Journal Apl. Prob.*, 11, 493-503.

Helmstetter, A. and Sornette, D., 2003. Predictability in the Epidemic-Type Aftershock Sequence model of interacting triggered seismicity, *J. Geophys. Res.*, 108 (B10), 2482; doi:10.1029/2003JB002485.

Hergarten, S. and Krenn, R., 2011. Synchronization and desynchronization in the Olami-Feder-Christensen earthquake model and potential implications for real seismicity, Nonlin. Processes Geophys., 18, 635–642; doi:10.5194/npg-18-635-2011.

Jones, L.M, 1988. Focal Mechanisms and the state of San Andreas Fault in Southern California, *J. Geophys. Res.*, 93 (B8), 8869-8891.

Kagan, Y.Y., 2002. Aftershock zone scaling, *Bull. Seismol. Soc. Am.,* 92 (2), 641-655.

Lay, T. and Wallace, T. C., 1995. *Modern Global Seismology*, Academic Press, New York, pp. 383-387.

Lise, S. and Paczuski, M., 2002. A Nonconservative Earthquake Model of Self-Organized Criticality on a Random Graph, Phys. Rev. Lett., 88 (22), 228301; doi: 10.1103/PhysRevLett.88.228301

Marsan, D. and Lengliné, O., 2008. Extending earthquakes's reach through cascading, *Science*, 319, 1076; doi: 10.1126/science.1148783.

Martinez, M.D., Lana, X., Posadas, A.M. and Pujades, L., 2005. Statistical distribution of elapsed times and distances of seismic events: the case of the Southern Spain seismic catalogue, *Nonlinear Proc. Geophys.*, 12, 235–244.

Marzocchi, W. and Lombardi, A. M., 2008. A double branching model for earthquake occurrence, *J. Geophys. Res.*, 113, B08317; doi:10.1029/2007JB005472.

McCaffrey, R., 2005. Block kinematics of the Pacific-North America plate boundary in the southwestern United States from inversion of GPS, seismological, and geologic data, *J. Geophys. Res.*, 110, B07401, doi: 10.1029/2004JB003307.

Michas, G., Vallianatos,F. and Sammonds, P., 2013. Non-extensivity and long-range correlations in the earthquake activity at the West Corinth rift (Greece), *Nonlin. Proc. Geoph.*, 20, 713-724.

Michas, G., Vallianatos, F. and Sammonds, P., 2015. Statistical mechanics and scaling of fault populations with increasing strain in the Corinth Rift, *Earth and Planetary Science Letters*, 431, 150–163; doi : 10.1016/j.epsl.2015.09.014.

Mignan, A., 2008. Non-Critical Precursory Accelerating Seismicity Theory (NC PAST) and limits of the power-law fit methodology. *Tectonophysics*, 452, 42–50. doi:10.1016/j.tecto.2008.02.010.

Molchan, G., 2005. Interevent time distribution in seismicity: A theoretical approach, *Pure appl. geophys.*, 162, 1135–1150; doi: 10.1007/s00024-004-2664-5.

Moré, J.J. and Sorensen, D.C., 1983. Computing a Trust Region Step, *SIAM Journal on Scientific and Statistical Computing*, 3, 553–572.

Newman, M. E. J., 1996. Self-Organized Criticality, Evolution and the Fossil Extinction Record, *Proc. Roy. Soc. Lond. B*, 263, 1605–1610.

Ogata, Y., 1988. Statistical models for earthquake occurrences and residual analysis for point processes, *J. Am. Stat. Assoc.*, 83 (401), 9-27.

Ogata, Y., 1998. Space-time point-process models for earthquake occurrences, *Ann. I. Stat. Math.*, 50 (2), 379-402.

Olami, Z., Feder, H. J. S. and Christensen, K., 1992. Self-Organized Criticality in a continuous, nonconservative cellular automaton modeling earthquakes, *Phys. Rev. Lett.*, 68, 1244–1247.

Papadakis, G., Vallianatos, F. and Sammonds, P., 2013. Evidence of Nonextensive Statistical Physics behaviour of the Hellenic Subduction Zone seismicity, *Tectonophysics*, 608, 1037-1048.

Papadakis, G., Vallianatos, F. and Sammonds, P., 2015. A Nonextensive Statistical Physics Analysis of the 1995 Kobe, Japan Earthquake, *Pure and Applied Geophysics*, 172 (7), 1923-1931.

Reasenberg, P. 1985. Second-order moment of central California seismicity, 1969-82, *J. Geophys. Res.*, 90, 5479, 5495.

Rhoades, D. A., 2007. Application of the EEPAS model to forecasting earthquakes of moderate magnitude in Southern California, *Seismol. Res. Lett.*, 78 (1), 110–115.

Rundle, J.B., Klein, W., Turcotte, D.L. and Malaud, B.D., 2000. Precursory seismic activation and critical point phenomena, *Pure appl. Geophys.*, 157, 2165-2182.

Saichev, A. and Sornette, D., 2013. Fertility Heterogeneity as a Mechanism for Power Law Distributions of Recurrence Times, *Physical Review E*, 97, 022815; also available at arXiv:1211.6062 [physics.geo-ph] (last access 20 October 2014).

Saleeby, J., Saleeby, Z., Nadin, E. and Maheo, G., 2009. Step-over in the structure controlling the regional west tilt of the Sierra Nevada microplate: eastern escarpment system to Kern Canyon system, *International Geology Review*, 51 (7-8), 634-669.

Sammis, C.G. and Sornette, D., 2001. Positive feedback, memory and the predictability of earthquakes, e-print at http://arXiv.org/abs/cond-mat/0107143v1; last accessed December 2015.

Schaff, D.P. and F. Waldhauser (2005), Waveform cross-correlation-based differential travel-time measurements at the Northern California Seismic Network, *Bull. Seism. Soc. Am.*, 95, 2446-2461.

Segou, M., T. Parsons, and W. Ellsworth, 2013. Comparative evaluation of physics-based and statistical forecasts in Northern California, *J. Geophys. Res. Solid Earth*, 118, doi:10.1002/2013JB010313.

Scherrer T.M, França G.S., Silva R., de Freitas D.B., Vilar C.S., 2015. Nonextensivity at the Circum-Pacific subduction zones – Preliminary studies, *Physica A: Statistical Mechanics and its Applications* , 426 63–71; doi: 10.1016/j.physa.2014.12.038.

Schoenball, M., N. C. Davatzes, and J. M. G. Glen, 2015. Differentiating induced and natural seismicity using space-time-magnitude statistics applied to the Coso Geothermal field, *Geophys.Res. Lett.*, 42, 6221–6228; doi:10.1002/2015GL064772.

Scholz, C., 2002. *The mechanics of earthquakes and faulting*, 2nd Edition, Cambrigde University Press, pp 198-211.

Silva, R., Franca, G.,S., Vilar, C.,S., Alcaniz, J.,S., 2006. Nonextensive models for earthquakes, *Physical Review E*, 73, 026102; doi:10.1103/PhysRevE.73.026102.

Sornette, A. and Sornette, D., 1989. Self-organized criticality and earthquakes, *Europhys. Lett.*, 9, 197-202.

Sornette, D., and Sammis, C.G, 1995. Complex critical exponents from renormalization group theory of earthquakes: Implications for earthquake predictions, *J. Phys. 1*, 5, 607-619.

Sornette, D., and Werner, M.J., 2009. Statistical Physics Approaches to Seismicity, in Complexity in Earthquakes, Tsunamis, and Volcanoes, and Forecast, W.H.K. Lee (Ed), in the *Encyclopedia of Complexity and Systems Science*, R. Meyers (Editor-in-chief), 7872-7891, Springer, ISBN: 978-0-387-755888-6; available at arXiv:0803.3756v2 [physics.geo-ph] (last access 20 October 2014).

Sotolongo-Costa, O. and Posadas, A., 2004. Tsalli's entropy: A non-extensive frequency-magnitude distribution of earthquakes. *Phys. Rev. Letters*, 92 (4), 048501; doi:10.1103/PhysRevLett.92.048501.

Steihaug, T., 1983. The Conjugate Gradient Method and Trust Regions in Large Scale Optimization, *SIAM J. Numer. Anal.*, 20, 626–637.

Talbi, A. and Yamazaki, F., 2010. A mixed model for earthquake interevent times, *J. Seismol*, 14, 289–307; doi: 10.1007/s10950-009-9166-y.

Telesca, L., 2010a. Nonextensive analysis of seismic sequences, Phys. Stat. Mech. Appl. 389, 1911–1914.

Telesca, L., 2010b. A nonextensive approach in investigating the seismicity of L'Aquila area (Central Italy), struck by the 6 April 2009 earthquake (M_L 5:8), Terra Nova, 22, 87–93.

Telesca, L., and Chen, C-C., 2010. Nonextensive analysis of crustal seismicity in Taiwan, Nat. Hazards Earth Syst. Sci., 10, 1293–1297.

Telesca, L., 2011. Tsallis-based nonextensive analysis of the Southern California seismicity. *Entropy*, 13, 1267-1280.

Telesca, L., 2012. Maximum Likelihood Estimation of the Nonextensive Parameters of the Earthquake Cumulative Magnitude Distribution, *Bull. Seismol. Soc. Am.*, 102, 886-891.

Touati, S., Naylor, M. and Main, I.G., 2009. Origin and Nonuniversality of the Earthquake Interevent Time Distribution, *Phys. Rev. Letters*, 102, 168501; doi: 10.1103/PhysRevLett.102.168501

Tsallis, C., 1988. Possible generalization of Boltzmann-Gibbs statistics, *J. Stat. Phys.*, 52, 479–487; doi:10.1007/BF01016429.

Tsallis, C., 2009. *Introduction to Nonextensive Statistical Mechanics: Approaching a Complex World*. Springer Verlag, Berlin, 378pp.

Uhrhammer B. R. A., Loper S. J., and Romanowicz B., 1996. Determination of local magnitude using BDSN Broadband Records, *Bull. Seism. Soc. Am.*, 86 (5), 1314-1330.

Utsu, T.; Ogata, Y.; Matsu'ura, R.S., 1995. The centenary of the Omori formula for a decay law of aftershock activity, *J. Phys. Earth*, 43, 1–33.

Vallianatos, F. and Sammond, P., 2011. A non-extensive statistics of the fault-population at the Valles Marineris extensional province, Mars, *Tectonophysics*, 509, 50–54; doi:10.1016/j.tecto.2011.06.001

Vallianatos, F. and Telesca, L. (Eds.), 2012. Statistical Mechanics in Earth Physics and Natural Hazards, *Acta Geophysica*, 60, 499–501.

Vallianatos, F., Michas, G., Papadakis, G. and Sammonds, P., 2012a. A non-extensive statistical physics view to the spatiotemporal properties of the June 1995, Aigion earthquake (M6.2) aftershock sequence (West Corinth Rift, Greece)", *Acta Geophysica*, 60 (3), 758-768.

Vallianatos, F. and Sammonds, P., 2013. Evidence of non-extensive statistical physics of the lithospheric instability approaching the 2004 Sumatran- Andaman and 2011 Honshu mega-earthquakes, *Tectonophysics*, doi: 10.1016/j.tecto.2013.01.009.

Vallianatos, F., Benson, P., Meredith, P. and Sammonds, P., 2012b. Experimental evidence of a non-extensive statistical physics behaviour of fracture in triaxially deformed Etna basalt using acoustic emissions , *Europhy. Let.*, 97, 58002 , doi: 10.1209/0295-5075/97/58002.

Vallianatos, F., Michas, G., Papadakis, G. and Tzanis, A., 2013a. Evidence of non-extensivity in the seismicity observed during the 2011–2012 unrest at the Santorini volcanic complex, Greece. *Nat. Hazards Earth Syst. Sci.*, 13, 177–185; doi:10.5194/nhess-13-177-2013.

Vallianatos, F., Karakostas, V. and Papadimitriou, E., 2013b. A Non-Extensive Statistical Physics View in the Spatiotemporal Properties of the 2003 (M_w6.2) Lefkada, Ionian Islands, Greece, aftershock sequence, *Pure and Applied Geophysics*, 171 (7), 1343–1354; doi:10.1007/s00024-013-0706-6.

Vallianatos F, Papadakis G, Michas G. 2016 Generalized statistical mechanics approaches to earthquakes and tectonics. *Proc. R. Soc. A*, 472: 20160497; doi: 10.1098/rspa.2016.0497.

van Stiphout, T., Zhuang J, and Marsan D., 2012, Seismicity declustering, Community Online Resource for Statistical Seismicity Analysis, doi: 10.5078/corssa-52382934. Available at http://www.corssa.org.

Waldhauser, F. and D.P. Schaff (2008), Large-scale relocation of two decades of Northern California seismicity using cross-correlation and double-difference methods, *J. Geophys. Res.*, 113, B08311, doi:10.1029/2007JB005479.

Wiemer, S., 2001. A software package to analyse seismicity: *ZMAP*, *Seismol. Res. Lett.*, 72 (2), 374-383.

Yang, X. S., 2001. Chaos in small-world networks, *Phys. Rev. E*, 63, 046206; DOI: 10.1103/PhysRevE.63.046206.

Yeats R., 2013. *Active Faults of the World*, Cambridge University Press.

Zhuang J., Ogata Y. and Vere-Jones D., 2002. Stochastic declustering of space-time earthquake occurrences, *J. Amer. Stat. Assoc.*, 97, 369-380.

Zhuang J., Ogata Y. and Vere-Jones D., 2004. Analyzing earthquake clustering features by using stochastic reconstruction, *J. Geophys. Res.*, 109 (B5), B05301; doi: 10.1029/2003JB002879.

Table 1. Summary of the variation of the entropic indices and *b*-values obtained from the analysis of North California full and declustered catalogues, as a function of threshold magnitude. $\overline{q}_T$ and $\overline{q}_M$ are the mean temporal and magnitude entropic indices respectively; $\sigma(q_T)$ and $\sigma(q_M)$ are the corresponding standard deviations. The last column lists *b*-values calculated with conventional techniques.

		Period	№ events	$\overline{q}_T$	$\sigma(q_T)$	q_T Range	$\overline{q}_M$	$\sigma(q_M)$	q_M Range	b_q range	b value
Comparative study	**NCSN**	1984-2011	6696	1.26	0.042	1.19-1.34	1.52	0.024	1.49-1.57	1.04-0.75	1.0-0.91
	DD		7465	1.18	0.086	1.04-1.33	1.52	0.026	1.49-1.58	1.04-0.73	1.1-0.96
Full NCSN		1968-2011	13345	1.33	0.033	1.29-1.40	1.51	0.024	1.49-1.56	1.04-0.79	1.01-0.92
		1968-1988	8298	1.38	0.038	1.35-1.44	1.50	0.006	1.49-1.51	1.04-0.96	1.01-0.91
		1990-2011	4677	1.20	0.057	1.12-1.26	1.48	0.008	1.48-1.5	1.08-1.00	1.02-0.96
Full nSAF		1968-2011	8443	1.29	0.044	1.22-1.35	1.51	0.030	1.48-1.56	1.12-0.78	1.15-0.95
		1968-1988	5736	1.51	0.074	1.40-1.62	1.51	0.027	1.48-1.56	1.12-0.78	1.18-0.95
		1990-2011	2391	1.13	0.043	1.05-1.20	1.48	0.012	1.46-1.49	1.12-1.00	1.13-0.99
Full SNR		1968-2011	4898	1.57	0.081	1.43-1.67	1.53	0.014	1.52-1.55	0.92-0.82	0.92-0.84
		1968-1988	2549	1.49	0.074	1.40-1.59	1.55	0.006	1.54-1.55	0.85-0.82	0.88-0.81
		1990-2011	2284	1.57	0.046	1.48-1.65	1.51	0.019	1.50-1.54	1.00-0.85	1.00-0.87
Declustered NCSN	$\phi_j \geq 70\%$	1968-2011	1963	1.45	0.060	1.34-1.55	1.53	0.013	1.51-1.55	0.96-0.82	0.95-0.75
	$\phi_j \geq 80\%$		1101	1.40	0.110	1.23-1.52	1.55	0.013	1.53-1.57	0.89-0.75	0.93-0.72
	$\phi_j \geq 90\%$		586	1.45	0.040	1.41-1.48	1.50	0.006	1.49-1.50	1.04-1.00	1.02-0.77
Declustered nSAF	$\phi_j \geq 70\%$	1968-2011	1196	1.48	0.080	1.41-1.60	1.51	0.014	1.49-1.54	1.04-0.85	0.99-0.78
	$\phi_j \geq 80\%$		667	1.47	0.09	1.37-1.58	1.52	0.006	1.51-1.52	0.96-0.92	0.99-0.75
	$\phi_j \geq 90\%$		370	1.56	NA	1.49-1.63	1.48	NA	1.48	1.08	1.15
Declustered SNR	$\phi_j \geq 70\%$	1968-2011	670	1.78	0.045	1.73-1.83	1.55	0.007	1.54-1.56	0.85-0.78	1.08-0.79
	$\phi_j \geq 80\%$		425	1.76	0.015	1.75-1.78	1.56	0.006	1.55-1.56	0.82-0.79	0.97-0.74

Table 2. Summary of the variation of the entropic indices and *b*-values obtained from the analysis of North California full and declustered catalogues, as a function of interevent distance. $\bar{q}_M$ is the mean magnitude entropic index; $\sigma(q_M)$ is the corresponding standard deviation.

Catalogue		**Period**	**№ events**	q_T **Range**		$\bar{q}_M$	$\sigma(q_M)$	q_M **Range**	b_q **Range**
				Δd **< 100km**	Δd **> 200km**				
Comparative Study	**NCSN**	1984-2011	6696	1.58 - 1.62	1.10 - 1.30	1.50	0.013	1.48 - 1.51	1.08 - 0.96
	DD		7465	1.58 - 1.62	1.10 - 1.30	1.49	0.016	1.46 - 1.51	1.17 - 0.96
Full NCSN		1968-2011	13345	1.55 - 1.40	1.28 - 1.42	1.49	0.026	1.46 - 1.51	1.17 - 0.96
		1968-1988	8298	1.40 - 1.70	~1.79	1.49	0.023	1.45 - 1.52	1.13 - 0.94
		1990-2011	4677	1.45 - 1.60	1.10 - 1.30	1.50	0.021	1.46 - 1.53	1.17 - 0.96
NCSN, declustered, $\phi_j \geq 70\%$		1968-2011	1963	1.86 – 1.34	1.38 – 1.66	1.51	0.041	1.47 – 1.57	1.13 - 0.76
Full nSAF		1968-2011	8443	1.62 - 1.55	1.29 - 1.49	1.48	0.017	1.46 - 1.51	1.17-0.96
		1968-1988	5736	1.58 - 1.55	1.38 - 1.66	1.49	0.014	1.48 - 1.51	1.12 - 1.00
		1990-2011	2391	1.60 – 1.22	1.14 – 1.39	1.47	0.026	1.45 - 1.50	1.12 - 1.00
Full SNR		1968-2011	4898	1.51 - 1.52	1.51 – 1.55	1.51	0.012	1.50 -1.53	1.00 - 0.92
		1968-1988	2549	1.33 - 1.84		1.54	0.03	1.54 - 1.55	0.85 - 0.82
		1990-2011	2284	1.57 - 1.73		1.48	0.026	1.46 - 1.52	1.17 - 0.92